

Article

# Simple and Powerful PCG Classification Method Based on Selection and Transfer Learning for Precision Medicine Application

Ahmed Barnawi <sup>1,\*</sup> , Mehrez Boulares <sup>1,2</sup> and Rim Somai <sup>3</sup>

<sup>1</sup> Information Technology Department, Faculty of Computing and Information Technology, King Abdulaziz University, Jeddah 21589, Saudi Arabia

<sup>2</sup> Research Laboratory of Technologies of Information and Communication and Electrical Engineering (LaTICE), Higher National School of Engineers of Tunis (ENSIT), University of Tunis, Tunis 1008, Tunisia

<sup>3</sup> ESPRIT School of Engineering, Tunis 2035, Tunisia

\* Correspondence: ambarnawi@kau.edu.sa

**Abstract:** The World Health Organization (WHO) highlights that cardiovascular diseases (CVDs) are one of the leading causes of death globally, with an estimated rise to over 23.6 million deaths by 2030. This alarming trend can be attributed to our unhealthy lifestyles and lack of attention towards early CVD diagnosis. Traditional cardiac auscultation, where a highly qualified cardiologist listens to the heart sounds, is a crucial diagnostic method, but not always feasible or affordable. Therefore, developing accessible and user-friendly CVD recognition solutions can encourage individuals to integrate regular heart screenings into their routine. Although many automatic CVD screening methods have been proposed, most of them rely on complex preprocessing steps and heart cycle segmentation processes. In this work, we introduce a simple and efficient approach for recognizing normal and abnormal PCG signals using Physionet data. We employ data selection techniques such as kernel density estimation (KDE) for signal duration extraction, signal-to-noise Ratio (SNR), and GMM clustering to improve the performance of 17 pretrained Keras CNN models. Our results indicate that using KDE to select the appropriate signal duration and fine-tuning the VGG19 model results in excellent classification performance with an overall accuracy of 0.97, sensitivity of 0.946, precision of 0.944, and specificity of 0.946.

**Keywords:** CVD classification; data selection; convolutional neural network; pretrained model; deep learning; transfer learning



**Citation:** Barnawi, A.; Boulares, M.; Somai, R. Simple and Powerful PCG Classification Method Based on Selection and Transfer Learning for Precision Medicine Application.

*Bioengineering* **2023**, *10*, 294.

<https://doi.org/10.3390/bioengineering10030294>

<https://doi.org/10.3390/bioengineering10030294>

Academic Editors: Pedro Miguel Rodrigues, João Paulo do Vale Madeiro and João Alexandre Lobo Marques

Received: 3 January 2023

Revised: 3 February 2023

Accepted: 15 February 2023

Published: 26 February 2023



**Copyright:** © 2023 by the authors. Licensee MDPI, Basel, Switzerland. This article is an open access article distributed under the terms and conditions of the Creative Commons Attribution (CC BY) license (<https://creativecommons.org/licenses/by/4.0/>).

## 1. Introduction

The World Health Organization (WHO) report [1] states that cardiovascular diseases (CVDs) are a leading cause of death, with 17.3 million deaths annually and an estimate of over 23.6 million deaths by 2030. Early and accurate CVD diagnosis can save lives by reducing the risk of heart failure [2]. One effective method for diagnosing CVDs is acoustic or PhonoCardioGram (PCG) pattern classification. This method recognizes abnormal blood flow sounds from heart valve dysfunction using acoustic signals. However, obtaining accurate results from classical CVD auscultation requires a highly skilled cardiologist. Screenings performed by primary care physicians or medical students have only 40% accuracy [3,4] and even experienced cardiologists have a screening accuracy of only 80% [3,5].

The neglect of regular heart screenings, due to unhealthy lifestyle habits, exacerbates the issue of CVDs. Making accessible and accurate CVD recognition solutions would encourage individuals to integrate regular heart screenings into their daily routine. Many studies have been conducted to diagnose CVDs using PCG signals, with a focus on improving classification results. However, these studies often rely on complex preprocessing steps,

optimized heart cycle segmentation, and combined classifier techniques applied to private or modified public PCG datasets. There is no objective comparative benchmark reference for future PCG-based CVD classification.

This paper addresses these issues by presenting a new CVD classification benchmark dedicated to the PCG Physionet dataset and a simple classification architecture based on PCG signal selection with CNN fine-tuning and transfer learning techniques.

The preprocessing of the acoustic signal prior to feeding it into a convolutional neural network (CNN) for classification can significantly impact the accuracy of the results. However, it is important to note that filtering may also remove essential information required by the CNN for proper classification, leading to a reduction in the signal's dynamic range and obscuring critical spectral features necessary for class differentiation. Our approach leverages strategies that avoid harmful filtering while still improving performance. By carefully selecting the training samples based on sample length and/or signal-to-noise ratio in the preprocessing phase, we have demonstrated the ability to significantly enhance the accuracy of the classification results.

The paper is organized as follows. In Section 2, we present some related work. In Section 3, we introduce the dataset setting and the different data selection methods. In Section 4, we present our classification model. In Section 5, experimental results are presented. In Section 6, we conclude the paper and indicate future and related research directions.

### *Contributions*

Our research focuses on the classification of normal and abnormal PhonoCardioGram (PCG) signals from the Physionet dataset using Convolutional Neural Network (CNN) technology. Our work presents two main contributions:

1. Development of a common benchmark for Physionet PCG dataset based on CNN transfer learning and fine-tuning techniques. This includes the presentation of classification results such as accuracy, sensitivity, specificity, and precision based on raw Physionet data.
2. Proposal of a simple and effective classification architecture without any preprocessing steps. Our approach is based on a simple PCG data selection technique to improve the normal and abnormal Physionet signal classification results using CNN technology.

## **2. Related Works**

Automatic classification of Cardiovascular Diseases (CVDs) is considered a challenging task due to the difficulty in acquiring a large labeled PCG dataset that covers the majority of CVDs. Despite these difficulties, numerous studies have been conducted in recent years. One such study by Grzegorzczak et al. [6] used a hidden Markov model for automatic PCG segmentation and neural networks for PCG signal training. The authors tested their approach on the Physionet dataset [7] and applied pretreatment to eliminate abnormal PCG records. They achieved a classification result with a specificity of 0.76 and a sensitivity of 0.81.

The study by Nouraei et al. in [8] examined the effect of unsupervised clustering strategies, including hierarchical clustering, K-prototype, and partitioning around medoids (PAM), on identifying distinct clusters in patients with Heart failure with preserved ejection (HFpEF) using a mixed dataset of patients. Through the examination of subsets of patients with HFpEF with different long-term outcomes or mortality, they were able to obtain six distinct results.

In [9], the authors conducted a comprehensive review of the relationship between artificial intelligence and COVID-19, citing various COVID-19 detection methods, diagnostic technologies, and surveillance approaches such as fractional multichannel exponent moments (FrMEMs) to extract features from X-ray images [10] and potential neutralizing antibodies discovered for the COVID-19 virus [11]. They also discussed the use of multi-layer perceptron, linear regression, and vector autoregression to understand the spread of the virus across the country [12].

Similarly, Chintalapudi et al. in [13] investigated the importance of utilizing machine learning techniques such as cascaded neural network models, recurrent neural networks (RNN), multilayer perception (MLP), and long short-term memory (LSTM) in the correct diagnosis of Parkinson's disease (PD).

We can also cite the work of [14] who proposed a public challenge based on the Physionet PCG dataset to improve the recognition score, which was initially 0.71 (sensitivity = 0.65, specificity = 0.76). During the competition, 48 teams submitted 348 open source entries and the highest score achieved was 0.86 (sensitivity = 0.94, specificity = 0.78). In the work of [15], the authors proposed a CVD classification technique using the Physionet dataset, which consisted of only 400 heart sound recordings. They relied on the time and frequency domain transformation of the phonocardiogram signal and used a logistic regression hidden semi-Markov model for PCG segmentation. For the classification task, they used and compared three different classifiers: support vector machines, convolutional neural network, and random forest.

In the study of [16], the authors proposed a classification method for cardiovascular diseases (CVD) using deep convolutional neural networks (CNNs) and time/frequency representations of the signals. In the work of [17], the authors used AdaBoost and CNNs to classify normal and abnormal PCG signals from the Physionet dataset. They achieved a sensitivity, specificity, and overall score of 0.9424, 0.7781, and 0.8602 respectively. In [18], the authors proposed a CVD classification based on preprocessing, feature extraction, and training with the Physionet dataset. They used neural networks to classify normal and abnormal signals and obtained a sensitivity of 0.812 and a specificity of 0.860 with an overall accuracy of 0.836.

The study in [19] used the Physionet dataset to perform anomaly detection using signal-to-noise ratio (SNR) and 1D Convolutional Neural Networks. In [20], the researchers presented a heart sound classification technique using multidomain features instead of heartbeat segmentation. They achieved an accuracy of 92.47% with improved sensitivity of 94.08% and specificity of 91.95%. The researchers in [20] used a Butterworth bandpass filter and a pretrained CNN model for CVD classification. In [21], the authors used deep neural network architectures and one-dimensional convolutional neural networks (1D-CNN) with a feed-forward neural network (F-NN) to classify normal and abnormal PCG signals from the Physionet dataset.

In the work of [22], the authors used Logistic Regression-Hsmm for PCG segmentation and feature extraction for CVD classification of normal and abnormal PCG signals from the Physionet dataset. They obtained an accuracy of 79%. In the study of [23], the authors used a pretrained CNN model (AlexNet) and achieved 87% recognition accuracy. The study in [24] aimed to use a nonlinear autoregressive network of exogenous inputs (NARX) for normal/abnormal classification of PCG signals from Physionet. In [25], the authors proposed a deep CNNs framework for heart acoustic classification using short segments of individual heartbeats. They used a 1D-CNN to learn features from raw heartbeats and a 2D-CNN to take inputs from two-dimensional time-frequency features.

### 3. Dataset

In this section, two different PCG datasets are presented. First, the raw Physionet dataset without any data selection process is described. Then, three different data selection methods applied on the original dataset are presented. The goal is to experiment with the impact of selection on the classification results.

#### 3.1. Raw Dataset

The publicly available Physionet dataset [14] is a not balanced PCG dataset which contains 665 normal sample and 2575 abnormal sample in WAV format. As shown in Figure 1, the majority of PCG samples are concentrated in the duration range between 8 and 40 s for normal and abnormal class.

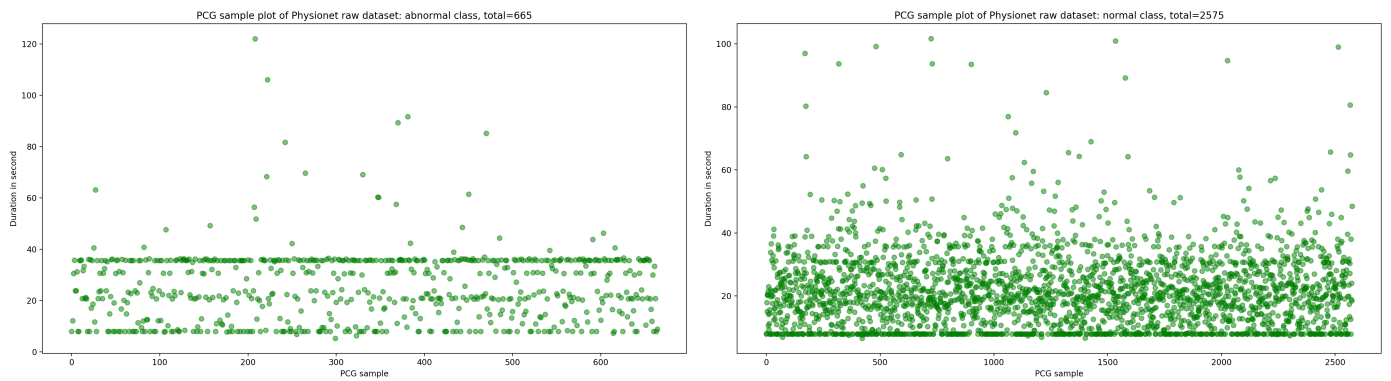


**Figure 1.** An overview of normal and abnormal sample distribution in function of duration in second.

If we look at Figure 2, we can deduce that for abnormal class, the highest density of PCG samples is defined at duration 35 s. Concerning the normal class, we can also deduce that the largest concentration of PCG samples are in signal duration 20 s.

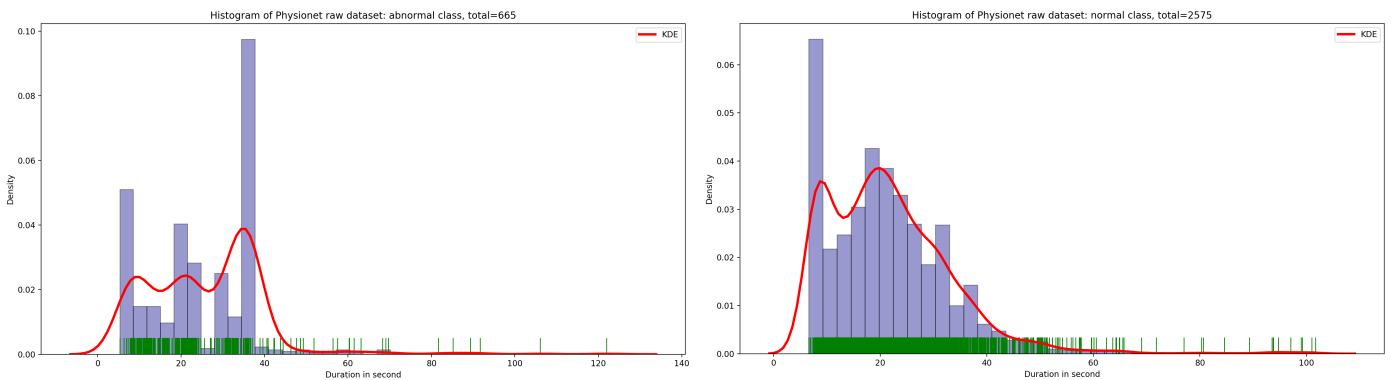


**Figure 2.** An overview of the kernel density estimation function using Gaussian kernel for normal and abnormal classes.

Concerning the signal-to-noise ratio (SNR) sample distribution in the function of density (as seen in Figure 3), we can deduce that the highest KDE value of SNR for normal and abnormal classes is zero. This means that the majority of Physionet PCG samples are approximately clean with an acceptable noise signal.

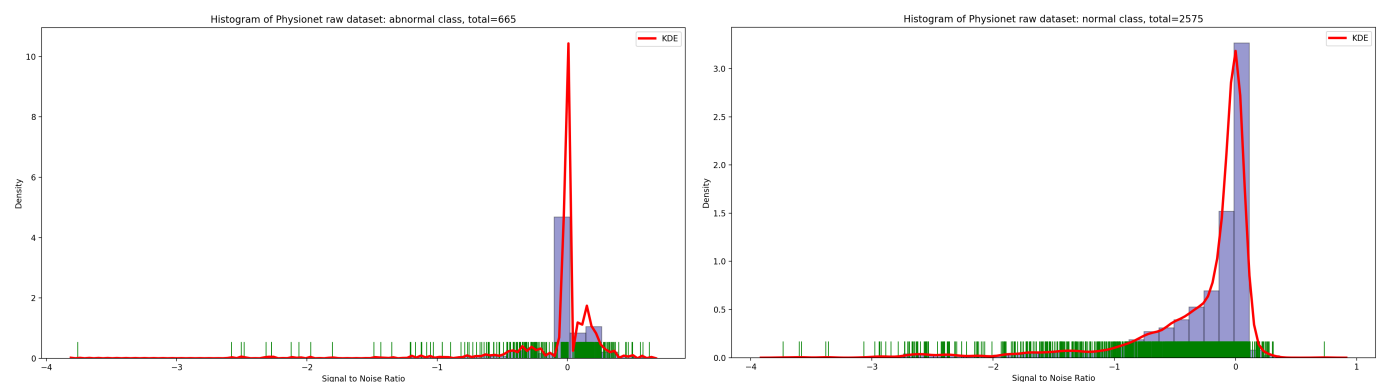


**Figure 3.** Signal-to-noise ratio in function of density related to normal and abnormal classes.

In the same manner, if we look at the Figure 4, it is visually clear that the highest concentration of PCG sample distribution related to normal and abnormal classes in function of SNR is approximately zero.

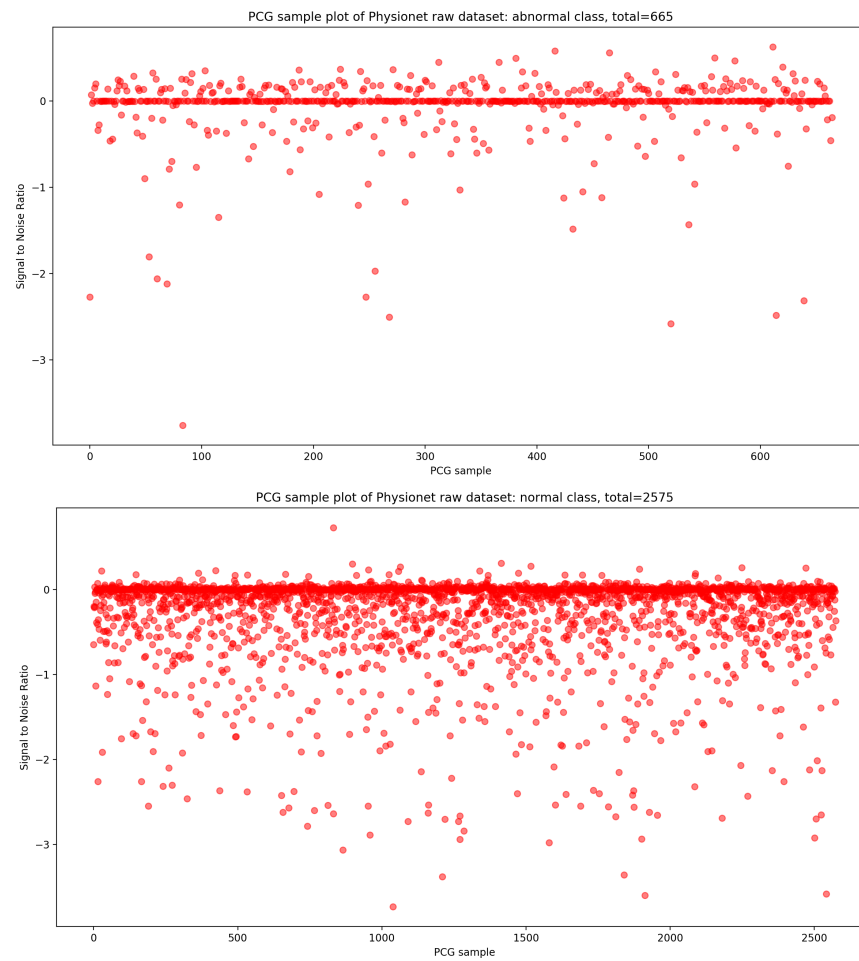


**Figure 4.** PCG sample distribution in function of signal-to-noise ratio of normal and abnormal classes.

### 3.2. PCG Data Selection

Based on the different results issued in the previous subsection, in this subsection, we present three main data selection process: data selection based on KDE for optimal signal duration determination, data selection based on optimal SNR, and data selection based on clustering. Notice that we will experiment the impact of these three data selection process on the classification results in the experimentation section.

#### 3.2.1. Data Selection Based on Kernel Density Estimation for Optimal Signal Duration Determination

Kernel density estimation (KDE) [26] is a non-parametric method for estimating the probability density function of a random variable. Given a set of points  $X_i$  with  $i = 1 \dots n$  in a  $d$  dimension space  $R^d$ , the kernel multivariate density estimation is obtained with a kernel  $K(x)$  and with window width  $h$  as following:

$$\hat{f}(x) = \frac{1}{nh^d} \sum_{i=1}^n K\left(\frac{|X_i - x|}{h}\right) \tag{1}$$

With  $K(u)$ : is a kernel function (using a Gaussian kernel (Formula (2))). The estimator  $\hat{f}(x)$  determines the percentage of observations closest to a given  $x$ . If there are several observations close to  $x$  then  $\hat{f}(x)$  widens. Conversely, if there are only a few  $X_i$  close to  $x$

then  $\hat{f}(x)$  remains weak. In other words, the  $h$  parameter of the Equation (1), determines the degree of smoothing of the KDE function.

$$k(u) = e^{-\frac{u^2}{2\sigma^2}} \tag{2}$$

Based on the discovery issued from the KDE curve shown in Figure 2, the idea is to select all the PCG samples for normal classes with signal duration equal to 20 s and 35 s for abnormal class. As seen in Figure 5, after applying this simple selection process, we obtain 238 PCG samples from abnormal class and 1291 PCG samples from normal class. If we look at the Figures 6 and 7, the obtained PCG samples after the KDE duration selection process for normal and abnormal classes have acceptable SNR values with a high SNR concentration, very close to zero.

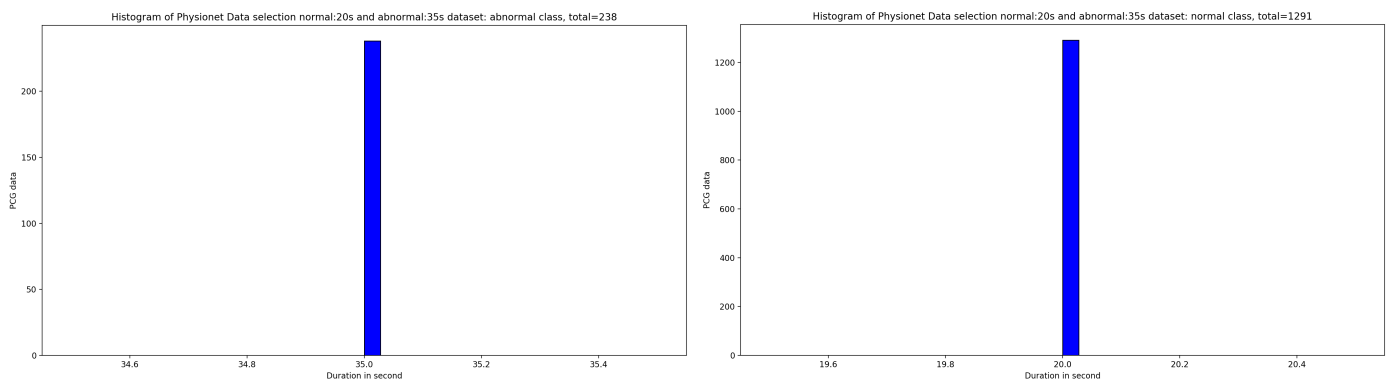


**Figure 5.** An overview of the PCG sample distribution in function of duration after selecting samples: 35 s from abnormal class and 20 s from normal class.

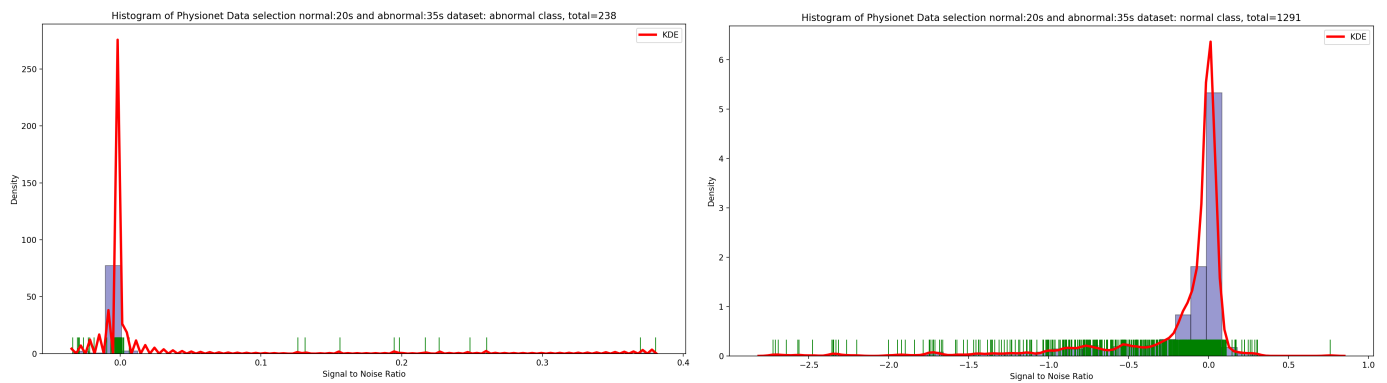


**Figure 6.** An overview of the SNR distribution in function of KDE density related to normal and abnormal samples after applying the KDE duration selection process.

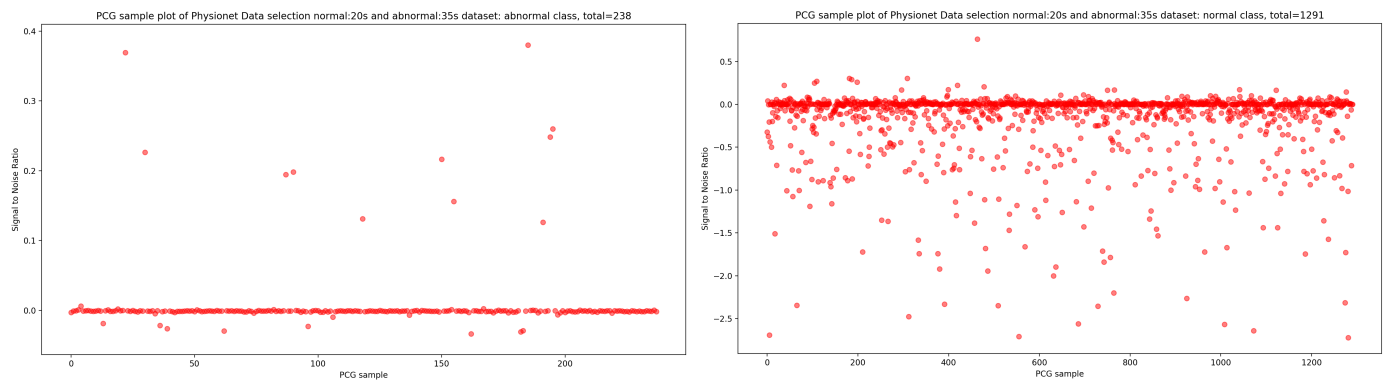


**Figure 7.** The PCG sample distribution in function of SNR of normal and abnormal classes after KDE duration selection process.

### 3.2.2. Data Selection Based on Optimal SNR

Signal-to-noise ratio (SNR) is defined as the ratio of signal power to the background noise power [27]. Based on the analysis of Figures 3 and 4, which show the highest concentration of SNR related to PCG samples for both normal and abnormal classes, we decided to select PCG samples with SNR greater than or equal to zero. As a result of this selection process, we obtained 221 PCG samples for the abnormal class and 822 PCG samples for the normal class, as shown in Figure 8. Additionally, Figures 9–11 provide an overview of the PCG sample distribution in terms of duration after the data selection process with SNR greater than or equal to 0, the KDE curve of PCG samples related to normal and abnormal classes in terms of duration after the SNR greater than or equal to zero in the data selection process, and the PCG sample distribution of normal and abnormal classes in terms of SNR greater than or equal to zero.

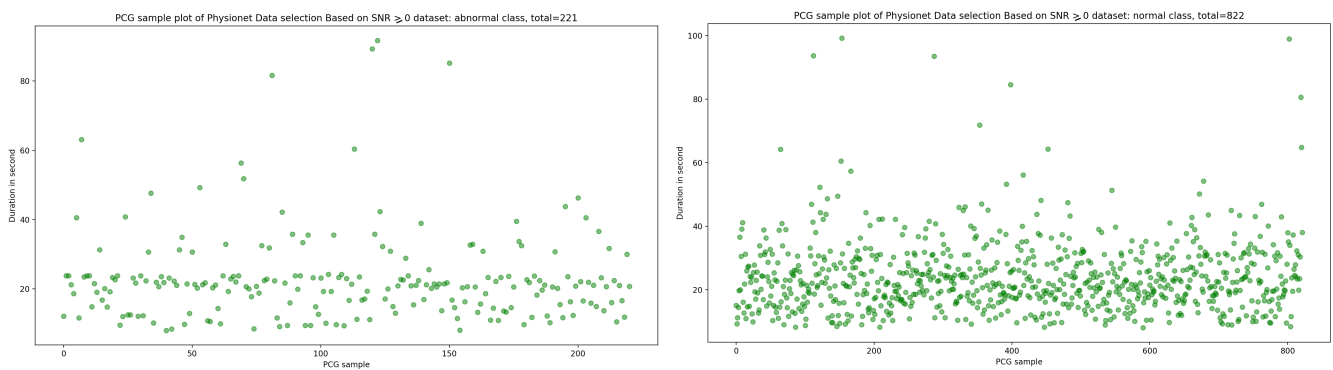


**Figure 8.** PCG sample distribution in function of duration after SNR greater than or equal to 0 in data selection process.

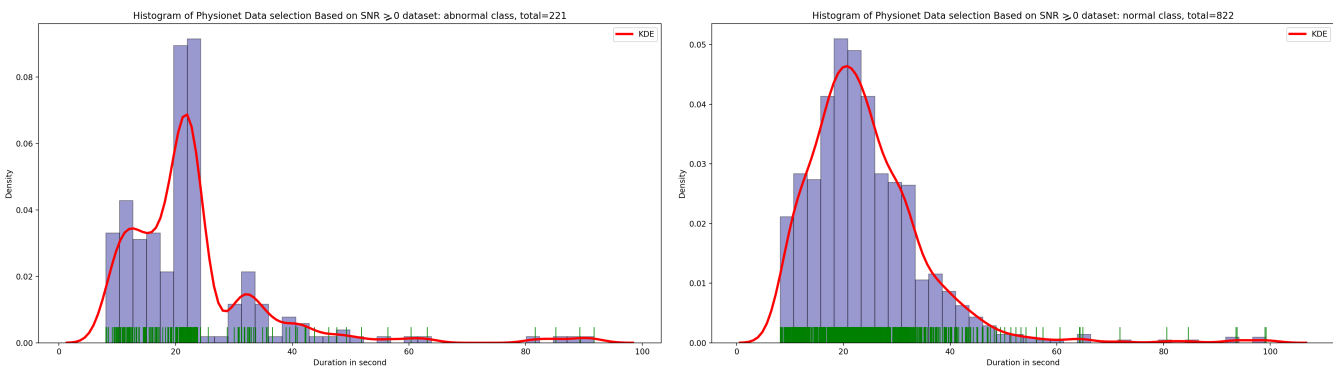


**Figure 9.** KDE curve of PCG samples related to normal and abnormal classes in function of duration after SNR greater than or equal to 0 in data selection process.

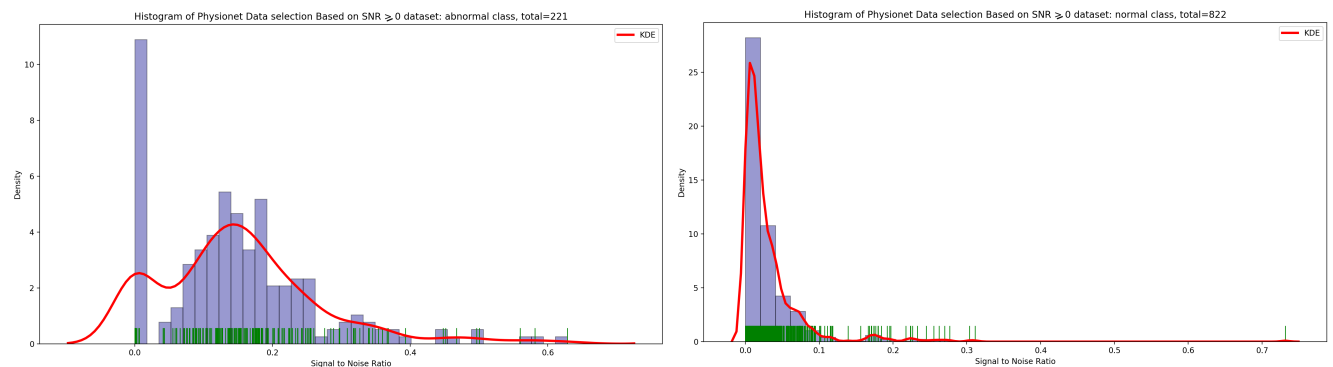


**Figure 10.** KDE curve of PCG samples related to normal and abnormal classes in function of SNR greater than or equal to 0.

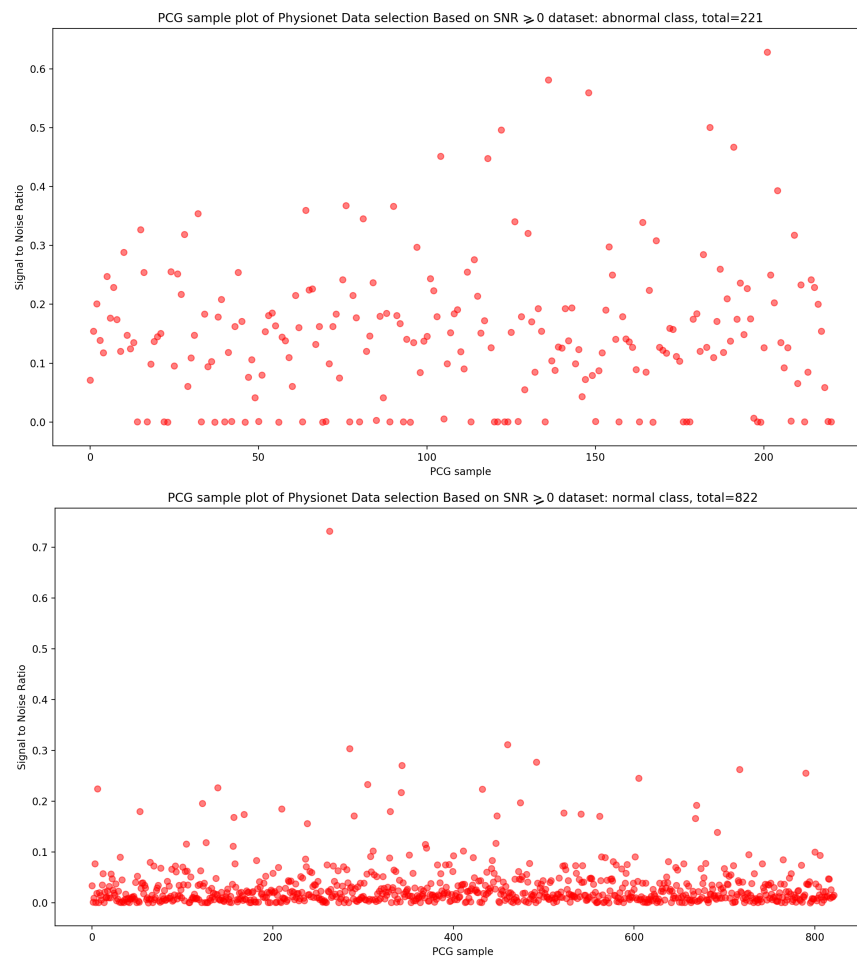


**Figure 11.** PCG samples distribution of normal and abnormal classes in function of SNR greater than or equal to 0.

### 3.2.3. Data Selection Based on Clustering

In this part, we chose to use biclustering as our data selection process. The main idea behind biclustering data selection is to suppose that the highest dense cluster constitutes our useful PCG data. In other words, we discard the remaining noise cluster and we preserve only the PCG samples belonging to the big cluster.

For this aim, we have chosen the mixture Gaussian model (GMM) [28] which is a parametric unsupervised clustering model. This model is used for data partitioning into several groups according to the probabilities of belonging and association to each Gaussian characteristics. GMM is based on a mixture of Gaussian models relying on learning the laws of probability that generated the observation data  $x_n$  (see Equation (3)).

$$f(x_n|\theta_k) = \sum_{k=1}^M \pi_k N(x_n|\mu_k, \sigma_k^2) \tag{3}$$

$N(x_n|\mu_k, \sigma_k^2) = \frac{1}{(2\pi)^{d/2}\sigma^{1/2}} e^{-\frac{1}{2\sigma_k^2}(x_n-\mu_k)^2}$ ,  $\pi_k \in 1..M$  is the probability of belonging to a Gaussian  $k$ ;  $k \in 1..M$ ,  $\mu_k \in 1..M$  is the set of the  $M$  Gaussian averages,  $\sigma_k^2 \in 1..M$  the set of covariances matrices, and  $\theta_k = \pi_k, \mu_k, \sigma_k^2$ . Similarly, the multidimensional version of the Gaussian is as follows:  $N(x_n|\mu_k, \Sigma_k) = \frac{1}{(2\pi)^{d/2}|\Sigma_k|^{1/2}} e^{-\frac{1}{2}(x_n-\mu_k)^T-\Sigma_k^{-1}(x_n-\mu_k)}$ . The best-known method for estimating the GMM parameters ( $\pi_k, \mu_k$  and  $\sigma_k^2$ ), is the iterative method of maximum likelihood calculation (expectation-maximization algorithm or EM [29]). The EM algorithm could be defined through 3 steps:

- Step 1: Parameter initialization  $\theta_k : \pi_k, \mu_k, \sigma_k^2$
- Step 2: Repeat until convergence
- Estimation step: Calculation of conditional probabilities  $t_{ik}$  that the sample  $i$  comes from the Gaussian  $k$ .  $t_{(i,k)} = \frac{\pi_k N(x_i | \mu_k, \sigma_k^2)}{\sum_{j=1}^m \pi_k N(x_i | \mu_j, \sigma_j^2)}$  with  $j \in 1, \dots, m$ : the set of Gaussians.
- Maximization step : Update settings  $\theta_k^{estim} = \operatorname{argmax}_{\theta_k} (\theta_k, \theta_k^{old})$  and  $\pi_k^{estim} = \frac{1}{n} \sum_{i=1}^N t_{i,k}$ ,  $\sigma_k^{2estim} = \frac{\sum_{i=1}^N t_{i,k} (x_i - \mu_k^{estim})^2}{\sum_{i=1}^N t_{i,k}}$ ,  $\mu_k^{estim} = \frac{\sum_{i=1}^N t_{i,k} x_i}{\sum_{i=1}^N t_{i,k}}$

The time complexity of EM algorithm for GMM parameters estimation [28–31] is as following: If  $X$  : is the dataset size,  $M$ : the Gaussian number, and  $D$ : the dataset dimension. EM estimation step  $O(XMD + XM)$ . EM maximization step  $O(2XMD)$ .

As seen in Figure 12, the result of the selection process based on the highest dense cluster issued from GMM biclustering gives us a 334 PCG sample for the abnormal class and a 1626 PCG sample for the abnormal class. The KDE curve in the function of duration and SNR related to normal and abnormal PCG samples is shown, respectively, in Figures 13 and 14. Furthermore, Figure 15 gives us an overview of the KDE curve in function of SNR for normal and abnormal PCG classes after the GMM data selection process.

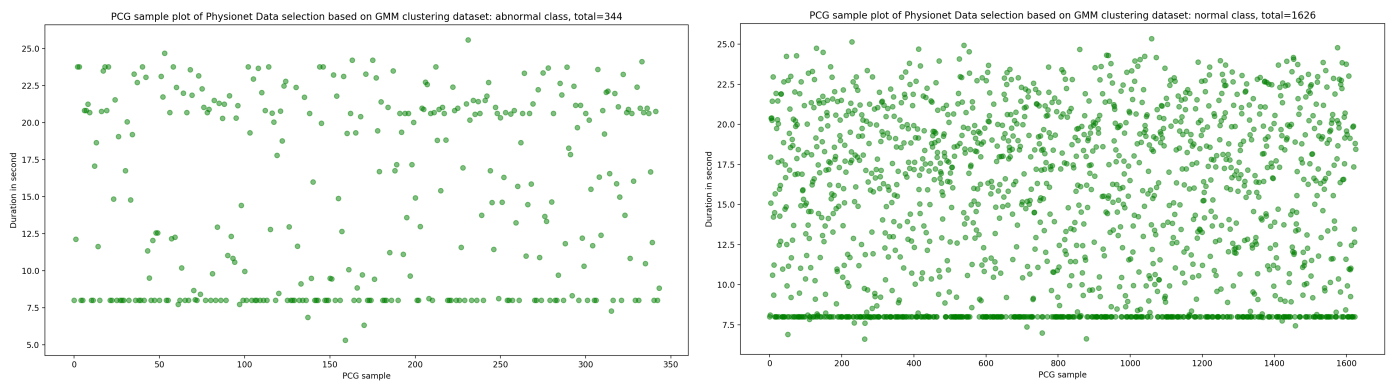


Figure 12. The PCG data distribution of normal and abnormal classes after selecting the highest dense cluster issued from GMM biclustering.

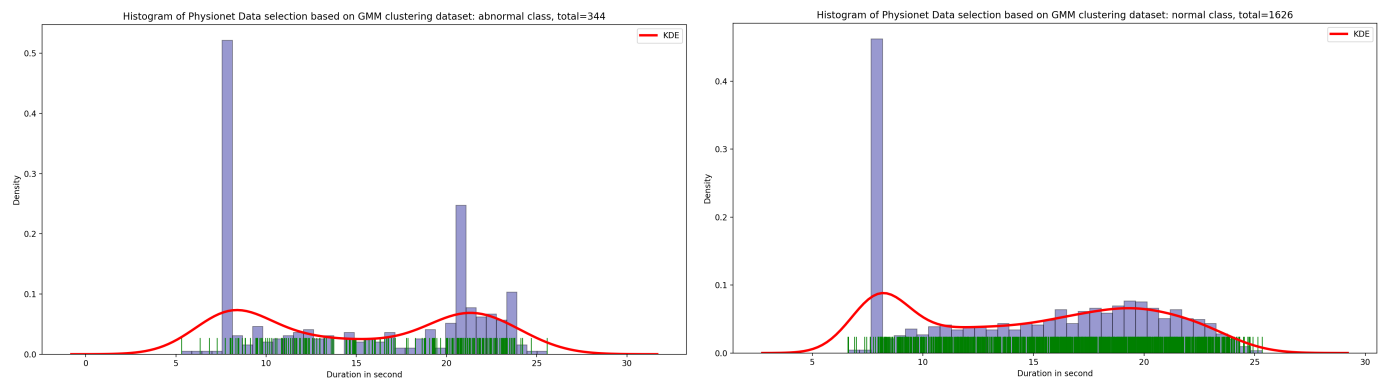
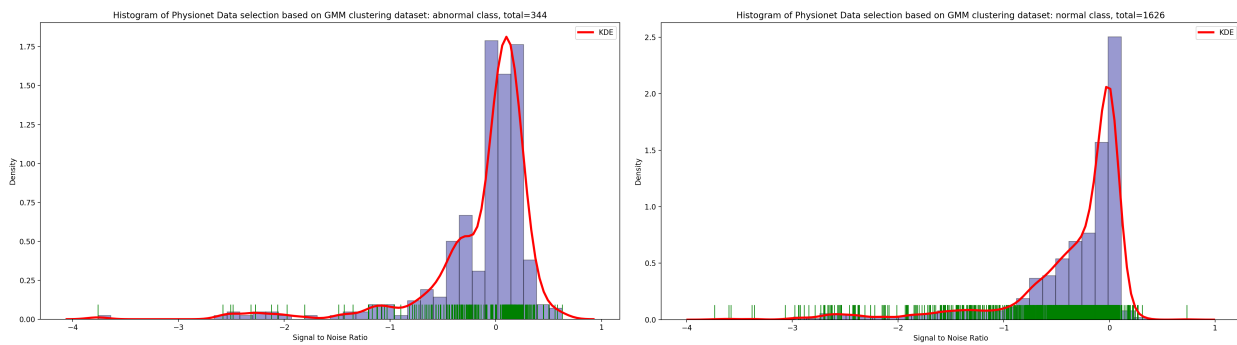
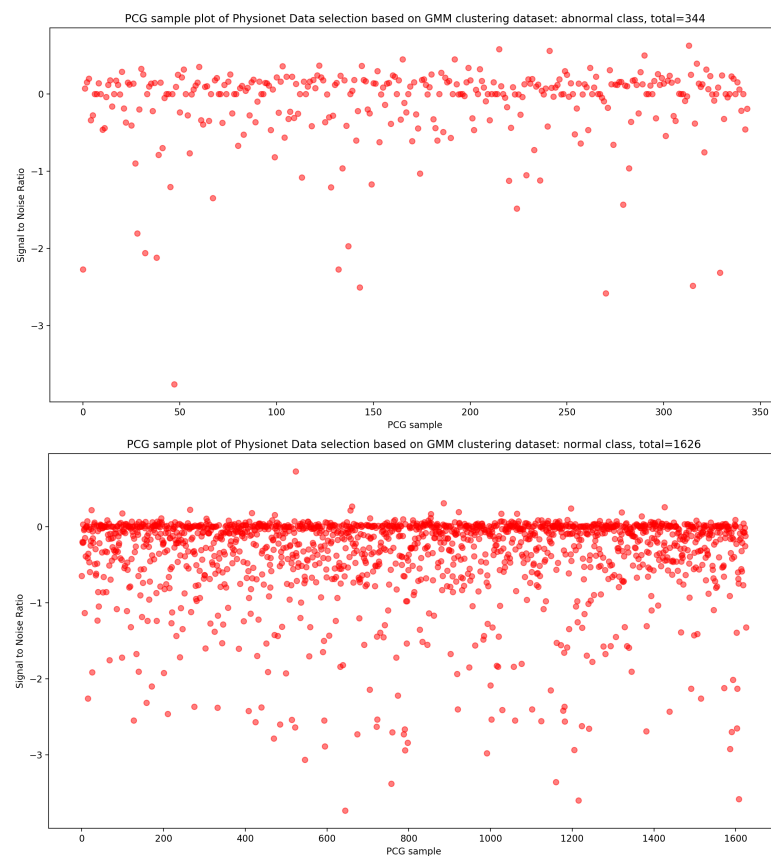


Figure 13. An overview of KDE curve in function of duration for normal and abnormal PCG classes after GMM data selection process.



**Figure 14.** An overview of KDE curve in function of SNR for normal and abnormal PCG classes after GMM data selection process.



**Figure 15.** PCG data distribution in function of SNR for normal and abnormal classes after GMM data selection process.

#### 4. The Process of Our CNN Benchmark

In this paper, we present a CNN classification system based on transfer learning and fine-tuning. Our system starts with the Physionet dataset, which we use to train the model. Figure 16 shows the architecture of our system, which is built on pretrained CNN models from ImageNet dataset. The first step involves transforming the wav PCG signals into mel spectrogram images using an FFT window of 1024 and a sample rate of 44,100. The second step defines the CNN parameters, including a two-class recognition, an input image size of width = 640 and height = 480, a batch size of 5, 30 epochs, and stochastic gradient descent as the optimizer with a learning rate of 0.0001. In the third step, we fine-tune the layers by using convolutional layers from the pretrained CNN models as feature extraction layers. Additionally, we add six layers including a GlobalAveragePooling2D layer for averaging and better representation of our training vector, three dense layers for the full connected

network, a BatchNormalization layer to limit covariate shift, and a dense layer with a sigmoid activation function to obtain a classification value between 0 and 1 (probability).

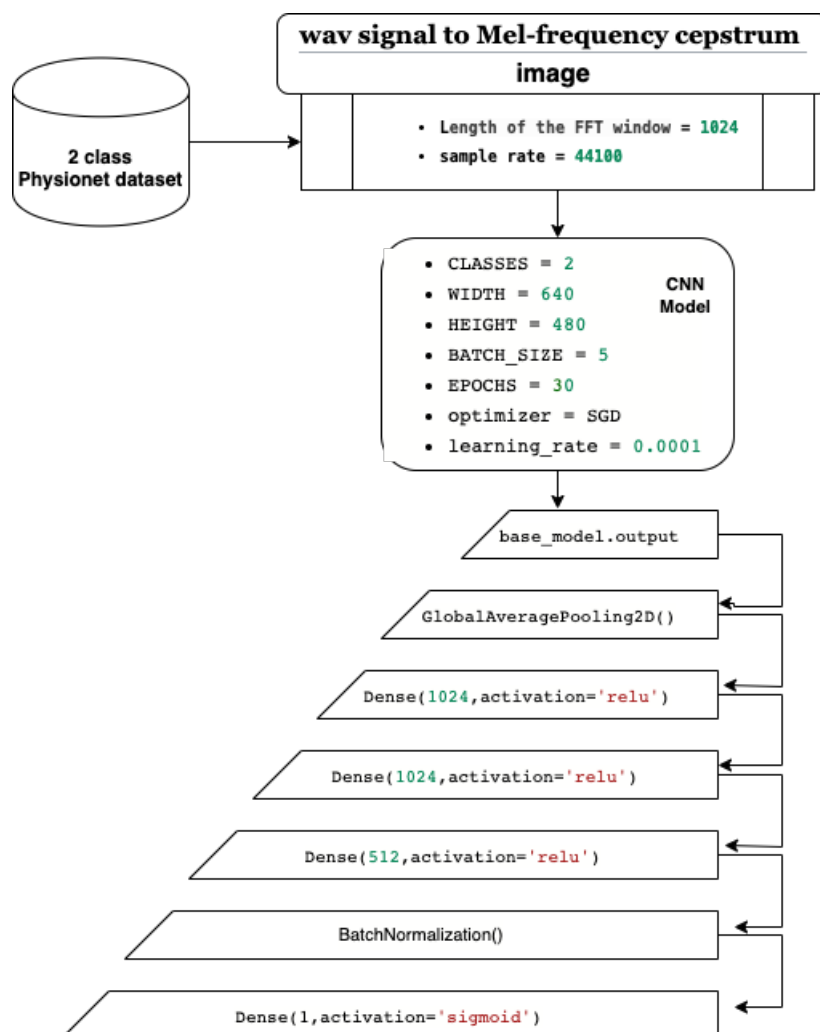


**Figure 16.** The architecture of our CNN system.

#### 4.1. Mel Spectrogram Representation

The fast Fourier transform is a powerful method to decompose acoustic signal amplitude over time into a multifrequency non periodic signal. However, if we need to represent the spectrum of these frequencies in function of time, we need to perform FFT over several windowed partitioned segments of the input signal. In fact, inspired by measured responses from the human auditory system, studies [32–35] have shown that humans perception does not perceive the frequencies on a linear scale. For this reason, a dedicated unit to transform frequencies was proposed by Stevens, Volkman, and Newmann in 1937. This is called the mel scale, which performs mathematical operation on frequencies to convert them to mel scale. In order to obtain the mel spectrogram, we perform the following steps (as seen in Figure 17):

1. Specify the signal into short frames.
2. Windowing in order to reduce spectral leakage.
3. Work out the discrete Fourier transformation.
4. Applying filter banks.
5. Applying the log of the spectrogram values to obtain the log filter-bank energies.
6. Applying discrete cosine transform to decorrelate the filter bank coefficients.

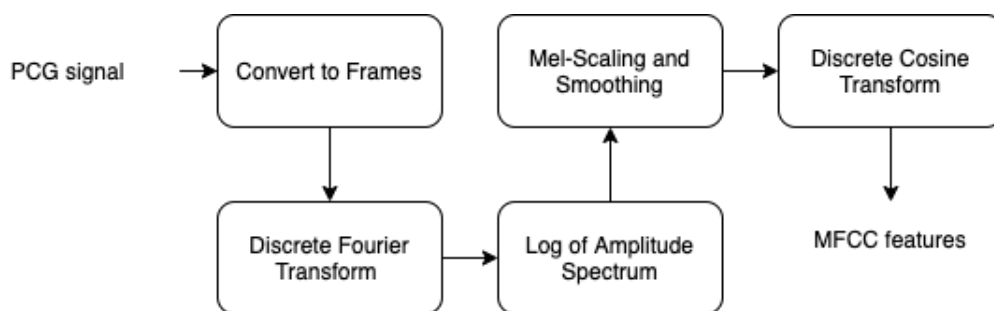


Figure 17. Mel spectrogram steps.

In this work, we have chosen MFCC signal by converting the output features into a png image, which will be applied to the CNN classifier. Figure 18 gives an overview of a normal and abnormal MFCC representation of the input PCG signal.

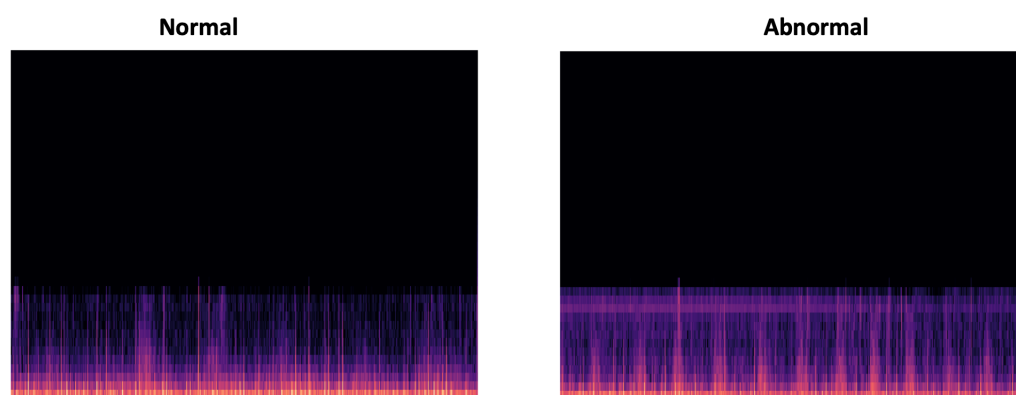


Figure 18. Overview of PCG spectrogram output (normal and abnormal, respectively).

#### 4.2. CNN Models

Recently, deep learning and more especially convolutional neural network (CNN) has trended as an image analysis and classification tool. In fact, many research has [36–39] have been conducted using CNN to propose neural network models that enable powerful image classification results. Moreover, it is known that CNNs can perform high-level feature extraction while tolerating image distortion conditions and illumination changes, and can provide invariance of image translation. For these reasons, we chose to adopt CNN as our PCG image trainer and classifier.

In fact, in 1998 LeCun [40] introduced the first CNN architecture, designed to recognize handwritten characters. Since the last decade, due to their satisfactory results in computer vision tasks such as face detection [41–43], handwritten recognition [44–46], and image classification [47–49], CNNs are the most-used technology for classifying images. However, in order to design new powerful CNN models, CNN requires large training datasets. Thanks to the knowledge-transfer technique also known as transfer learning appellation [50], it becomes possible to take the advantages of the already trained CNN models on ImageNet by applying some modifications called fine-tuning. Therefore, we can customize these pretrained CNN models in order to be trained on a small dataset without a huge drop in the classification results.

In our work, we used several pretrained CNN models to classify normal/abnormal PCG spectrogram images. Based on the small public dataset PhysioNet, we fine-tuned and trained the 17 pretrained Keras CNN models (see Table 1). We preserved the convolutional layers which will be used for feature extraction then the additional layers are added:

1. GlobalAveragePooling2D layer for averaging and better representation of our training vector.
2. Three dense layers to define our full connected network.

3. BatchNormalization layer to limit covariate shift by normalizing the activations of each layer.
4. Dense layer with sigmoid activation function in order to obtain classification values between 0 and 1 (probability).

Keras CNN models are trained on the following dataset using the Google Colab platform to allow the use of dedicated GPU facilities: 1×Tesla K80 , having 2496 CUDA cores, compute 3.7, 12 GB (11.439 GB Usable) GDDR5 VRAM:

1. Raw PhysioNet dataset.
2. PhysioNet dataset with data selection using KDE for duration extraction.
3. PhysioNet dataset with data selection using optimal SNR.
4. PhysioNet dataset with data selection using GMM biclustering.

**Table 1.** Keras CNN models.

Model	Citation	Layers	Size	Parameters
Xception	[51]	71	85 MB	44.6 million
VGG19	[52]	26	549 MB	143.6 million
VGG16	[52]	23	528 MB	138.3 million
ResNet152V2	[53]	-	98 MB	25.6 million
ResNet152	[53]	-	232 MB	60.4 million
ResNet101V2	[53]	-	171 MB	44.6 million
ResNet101	[53]	101	167 MB	44.6 million
ResNet50V2	[53]	-	98 MB	25.6 million
ResNet50	[53]	-	98 MB	25.6 million
NASNetMobile	[54]	-	20 MB	5.3 million
MobileNetV2	[55]	53	13 MB	3.5 million
MobileNet	[56]	88	16 MB	4.25 million
InceptionV3	[57]	48	89 MB	23.9 million
InceptionResNetV2	[58]	164	209 MB	55.9 million
DenseNet201	[59]	201	77 MB	20 million
DenseNet169	[59]	169	57 MB	14.3 million
DenseNet121	[59]	121	33 MB	8.06 million

## 5. Experiments and Results

The effect of selecting data on the accuracy of the classification is being studied. First, we concentrate on training and classifying CNN models using the raw dataset without any data selection. Next, we train our CNN models on the data that has been selected based on a 20 s duration for normal PCG signals and 35 s for abnormal PCG signals. Finally, we examine the impact of selecting data based on SNR greater than 0 in the third section. It is worth mentioning that all the classification results have been obtained by taking the average of the results from the three-fold cross validation.

### 5.1. Classification Using Raw Dataset

After performing CNN training on the raw Physionet dataset, we can notice that VGG19 gives the best classification results with accuracy = 0.854, sensitivity = 0.860, precision = 0.794, and specificity = 0.860 (as seen in Table 2).

**Table 2.** Average metric results related to the raw dataset.

Average	Accuracy	TPR (Sensitivity)	Precision (PPV)	TNR (Specificity)
VGG16	0.6	0.527	0.502	0.527
VGG19	<b>0.854</b>	<b>0.860</b>	<b>0.794</b>	<b>0.860</b>
Xception	0.783	0.797	0.714	0.797
ResNet152V2	0.659	0.679	0.665	0.679
ResNet152	0.580	0.689	0.634	0.689
ResNet101V2	0.282	0.537	0.575	0.537
ResNet101	0.404	0.585	0.596	0.585
ResNet50v2	0.792	0.702	0.702	0.702
ResNet50	0.538	0.624	0.638	0.624
NasNetMobile	0.619	0.496	0.347	0.496
MobileNetV2	0.435	0.476	0.460	0.476
MobileNet	0.558	0.595	0.653	0.595
Inceptionv3	0.676	0.758	0.673	0.758
InceptionResNetV2	0.825	0.807	0.748	0.807
DenseNet201	0.576	0.657	0.658	0.657
DenseNet169	0.704	0.771	0.715	0.771
DenseNet121	0.424	0.622	0.620	0.622

In addition, we can see that the classification results related to InceptionResNetV2 are close VGG19 with accuracy = 0.825, sensitivity = 0.807, precision = 0.748, and specificity = 0.807. Similarly, Figure 19 gives an overview of the validation and training curves related to VGG19 and InceptionResNetV2. If we look at Figure 20, we can see that, if we consider the training step duration, mobileNet is the fastest CNN model and ResNet101 is the lowest CNN model. On the other hand, we can see that despite the number of layer of VGG19 (best accuracy result) which is 26 (as seen in Table 1) compared to deeper architecture (such as DenseNet201 with 201 layers) VGG19 is slower than DenseNet201 and is ranked as the fourth-slowest CNN model in term of training time.

#### Classification Using Kernel Density Estimation as Data Selection Method for Signal Duration 20 s Normal and 35 s Abnormal

After performing data selection on Physionet through the use of signal duration extraction with 20 s for normal PCG signals and 35 s for abnormal PCG signals, we trained all the 17 pretrained CNN models (see Table 1 and we obtained the classification results presented in Table 3. We can notice that through the use of this simple data selection, we obtained an enhancement of all the classification results compared to those without any data selection. As seen in Table 3, we obtained an improvement of VGG19 accuracy from 0.854 (raw dataset) to 0.970, for sensitivity from 0.860 to 0.946, for precision from 0.794 to 0.944, and for specificity from 0.860 to 0.946. Similarly, Figure 21 gives an overview of the validation and training curves related to VGG19 and VGG16. In addition, as seen in Figure 22, the training phase related to VGG19 becomes faster (fourth position after mobilenet, inceptionV3 and resnet50) than the one without data selection. This means that this data selection method allows us to speed up the training phase related to VGG19. On the other hand, we performed an experimental test in order to argue the choice of 20 s and 35 s signal duration extraction, respectively, for normal and abnormal signals. In this test we chose a random signal duration extraction value equal to 50 s for normal and abnormal signals. The classification results related to this experiment is shown in Table 4. If we compare the classification results presented in Tables 3 and 4, we can see that for VGG19

(best model), the accuracy decreases from 0.970 to 0.870, sensitivity decreases from 0.946 to 0.851, precision decreases from 0.944 to 0.801, and specificity decreases from 0.946 to 0.851. All these results support the idea behind our duration selection method (explained in data selection based on kernel density estimation for optimal signal duration determination subsection).

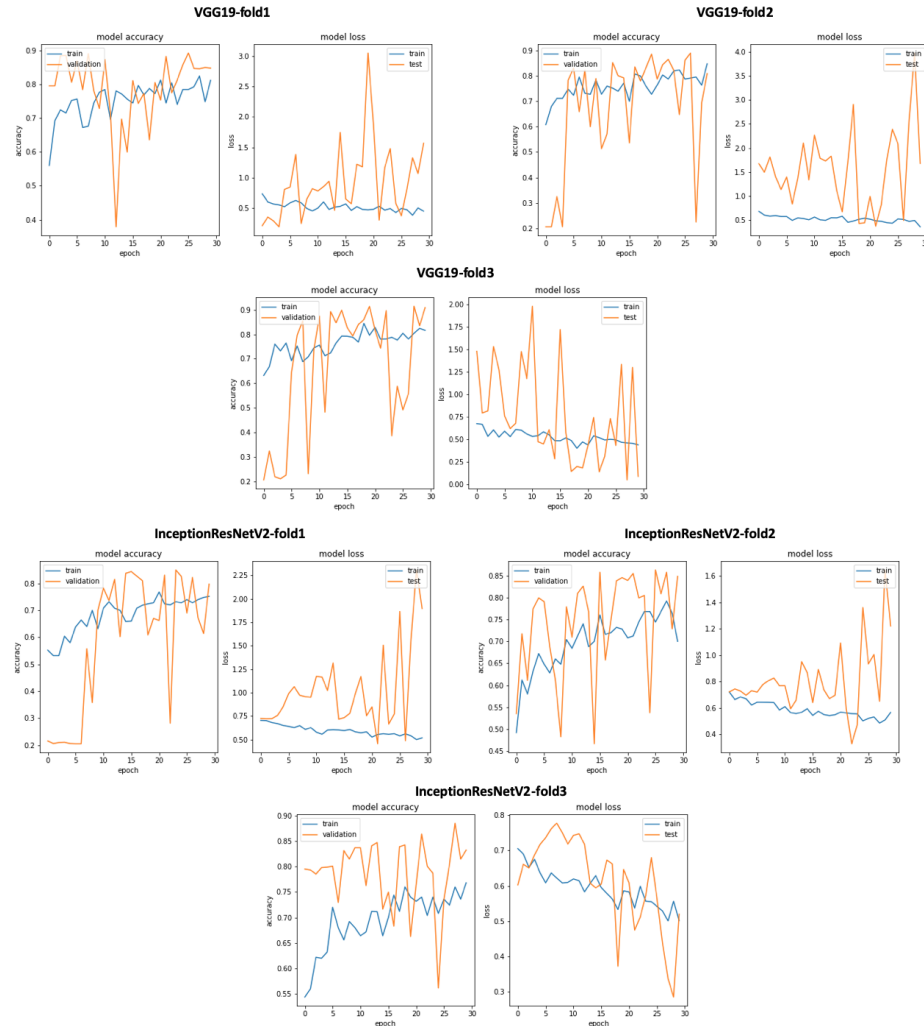


Figure 19. VGG19 and InceptionResNetV2 training and validation curves using raw dataset.

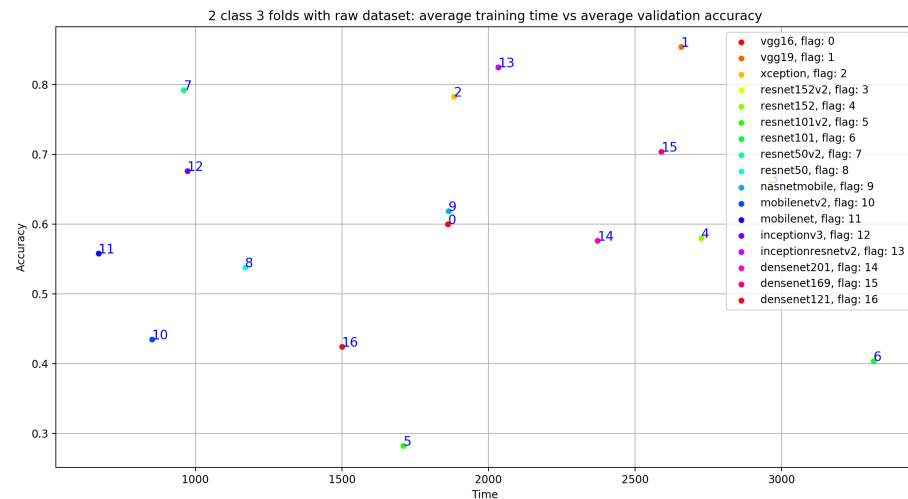


Figure 20. Training time vs. validation accuracy using raw dataset.

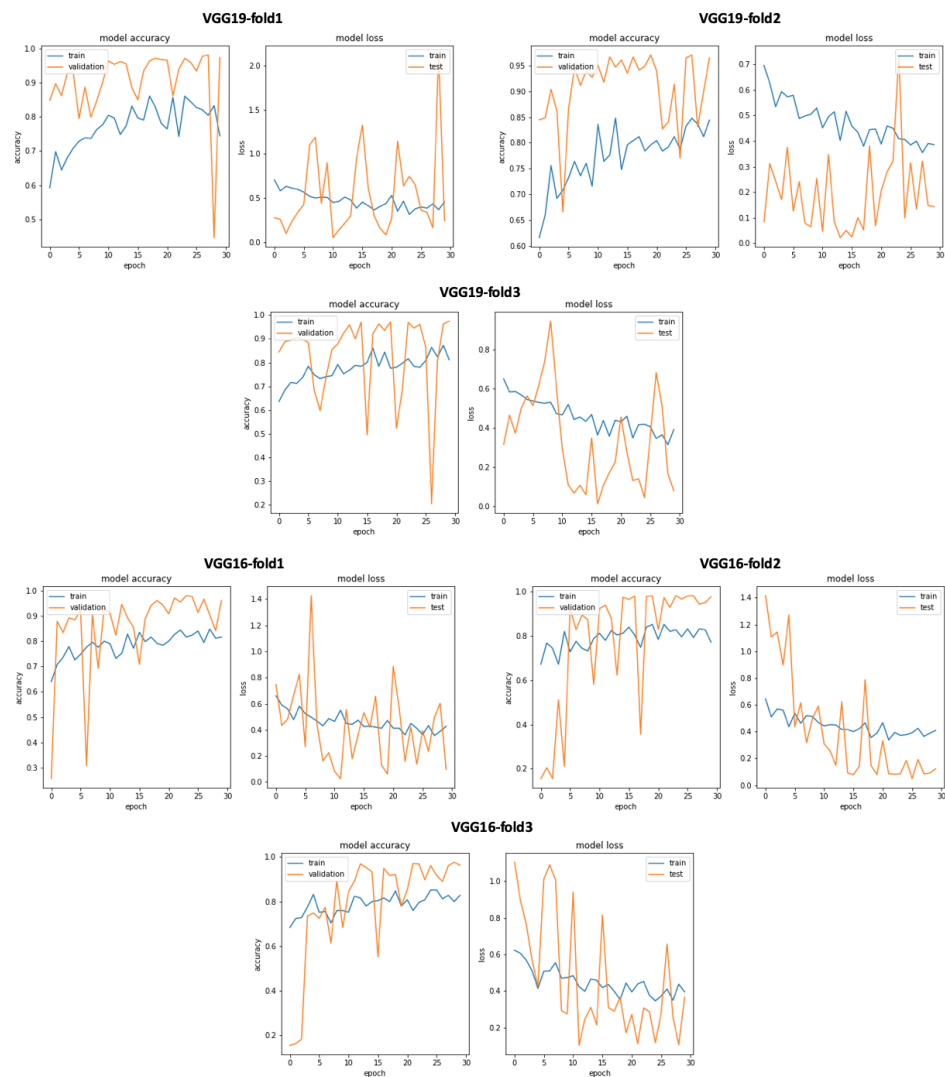


Figure 21. VGG19 and VGG16 training and validation curves using data selection based on KDE.

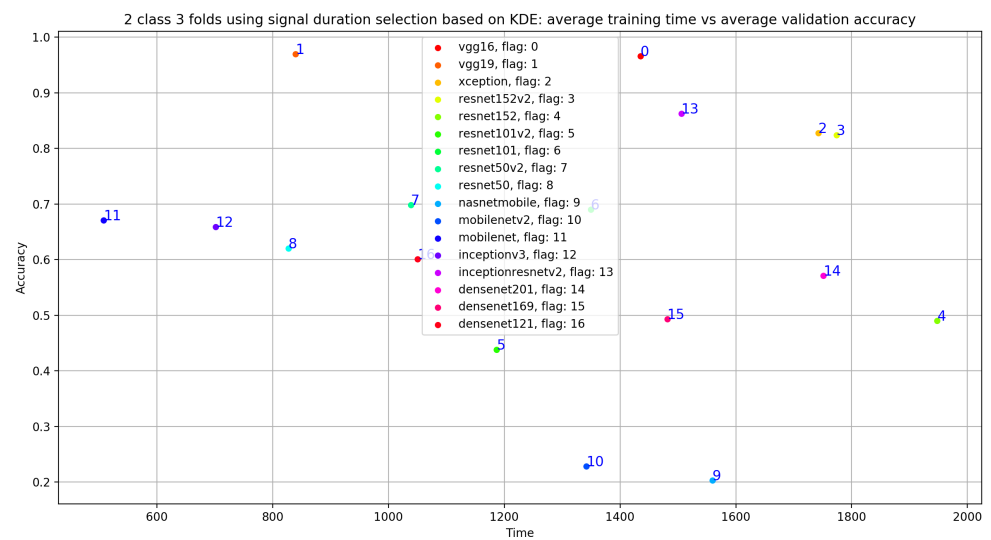


Figure 22. Training time vs. validation accuracy using signal-duration selection based on KDE.

**Table 3.** Average metric results related to KDE (duration = 20 s normal, duration = 35 s abnormal) datasets.

Average	Accuracy	TPR (Sensitivity)	Precision (PPV)	TNR (Specificity)
VGG16	0.966	0.930	0.946	0.930
VGG19	<b>0.970</b>	<b>0.946</b>	<b>0.944</b>	<b>0.946</b>
Xception	0.828	0.877	0.732	0.877
ResNet152V2	0.824	0.873	0.730	0.873
ResNet152	0.490	0.667	0.640	0.667
ResNet101V2	0.438	0.665	0.422	0.665
ResNet101	0.690	0.592	0.812	0.592
ResNet50v2	0.698	0.736	0.728	0.736
ResNet50	0.620	0.763	0.685	0.763
NasNetMobile	0.203	0.489	0.350	0.489
MobileNetV2	0.228	0.497	0.526	0.497
MobileNet	0.671	0.679	0.673	0.679
Inceptionv3	0.659	0.791	0.686	0.791
InceptionResNetV2	0.863	0.908	0.765	0.908
DenseNet201	0.571	0.725	0.719	0.725
DenseNet169	0.493	0.675	0.606	0.675
DenseNet121	0.601	0.734	0.714	0.734

**Table 4.** Average metric results related to duration = 50 s dataset.

Average	Accuracy	TPR (Sensitivity)	Precision (PPV)	TNR (Specificity)
VGG16	0.668	0.747	0.703	0.747
VGG19	<b>0.870</b>	<b>0.851</b>	<b>0.801</b>	<b>0.851</b>
Xception	0.702	0.781	0.689	0.781
ResNet152V2	0.501	0.669	0.636	0.669
ResNet152	0.785	0.677	0.687	0.677
ResNet101V2	0.457	0.628	0.606	0.628
ResNet101	0.600	0.616	0.674	0.616
ResNet50v2	0.433	0.626	0.611	0.626
ResNet50	0.473	0.581	0.636	0.581
NasNetMobile	0.451	0.494	0.329	0.494
MobileNetV2	0.576	0.535	0.541	0.535
MobileNet	0.562	0.680	0.657	0.680
Inceptionv3	0.751	0.740	0.729	0.740
InceptionResNetV2	0.667	0.687	0.687	0.687
DenseNet201	0.694	0.744	0.713	0.744
DenseNet169	0.609	0.703	0.699	0.703
DenseNet121	0.495	0.637	0.621	0.637

### 5.2. Classification Using Data Selection Based on Optimal SNR

The idea behind this data selection method is to select all the PCG signals with a signal-to-noise ratio greater than or equal to 0. In other words, we experiment the impact

of selecting signals with  $SNR \geq 0$  on the classification result without performing any preprocessing steps or denoising methods. After applying this data selection method, we trained all the 17 pretrained CNN models (Figure 23 gives an overview of training and validation curves related to VGG19, VGG16, DenseNet169, and InceptionResNetV2). As seen in Table 5, we obtained very good classification results with VGG19, VGG16, DenseNet169, and InceptionResNetV2. The best result was obtained with VGG19 (accuracy = 0.96, sensitivity = 0.943, precision = 0.94 and specificity = 0.943). This result is very close to the classification result obtained after applying data selection based on signal duration.

In fact, if we look at Figure 24, we notice that the VGG19 training time is at the fifth position compared to the fourth position obtained with VGG19, trained on 20 s and 35 s normal and abnormal PCG signals. In other words, the best results in term of training time and classification results was obtained using VGG19 trained on 20 s and 35 s normal and abnormal PCG signals.

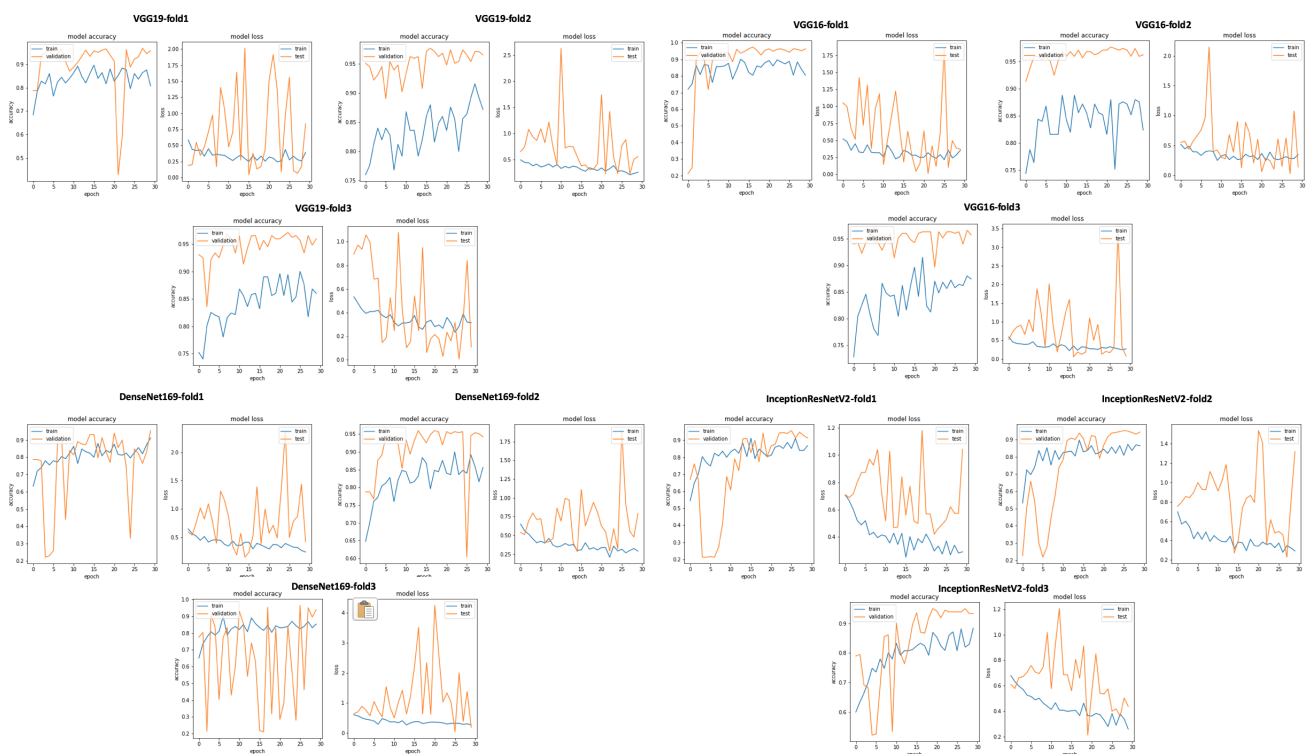


Figure 23. VGG19, VGG16, DenseNet169, and InceptionResNetV2 training and validation curves using data selection based on  $SNR \geq 0$ .

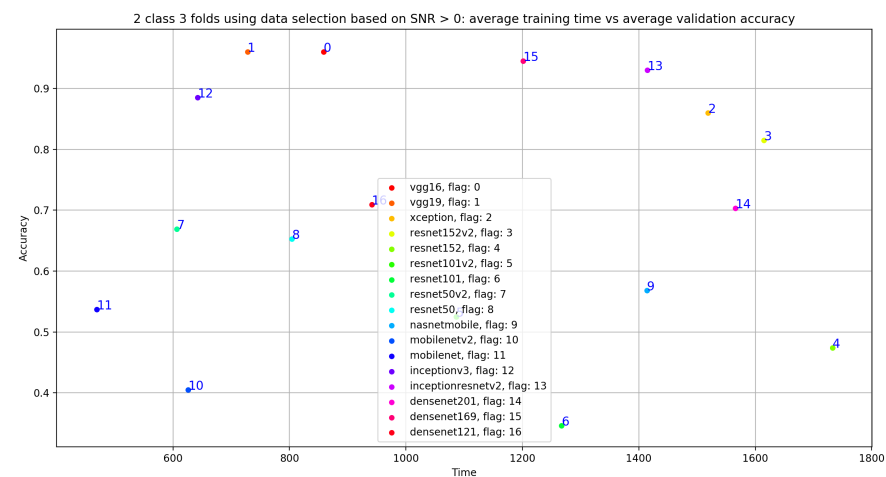


Figure 24. Training time vs. validation accuracy using data selection based on  $SNR \geq 0$ .

**Table 5.** Average metric results related to SNR  $\geq 0$  dataset.

Average	Accuracy	Sensitivity	Precision	Specificity
VGG16	0.960	0.938	0.944	0.938
VGG19	<b>0.960</b>	<b>0.943</b>	<b>0.940</b>	<b>0.943</b>
Xception	0.860	0.895	0.807	0.895
ResNet152V2	0.815	0.845	0.790	0.845
ResNet152	0.474	0.660	0.665	0.660
ResNet101V2	0.525	0.687	0.561	0.687
ResNet101	0.346	0.581	0.611	0.581
ResNet50v2	0.669	0.773	0.745	0.773
ResNet50	0.653	0.746	0.566	0.746
NasNetMobile	0.568	0.492	0.344	0.492
MobileNetV2	0.405	0.561	0.521	0.561
MobileNet	0.537	0.696	0.712	0.696
Inceptionv3	0.885	0.893	0.855	0.893
InceptionResNetV2	0.930	0.939	0.880	0.939
DenseNet201	0.703	0.789	0.612	0.789
DenseNet169	0.945	0.938	0.907	0.938
DenseNet121	0.709	0.800	0.810	0.800

### 5.2.1. Classification Using Clustering as Data Selection Method

In this subsection, we investigate the impact of selecting training data using unsupervised biclustering. We used GMM biclustering with the hypothesis to consider the cluster with the maximum number of sample as our training data. As shown in Table 6 and in Figure 25, we obtained good classification results compared to results without using any data selection method. However, if we compare with the previous results, we can conclude that the best results are obtained using signal selection, based on duration 20 s for normal and 35 s for abnormal PCG data. In this configuration, VGG16 gives the best classification metrics compared to the remaining 16 CNN models with an acceptable training time (sixth position) as seen in Figure 26.

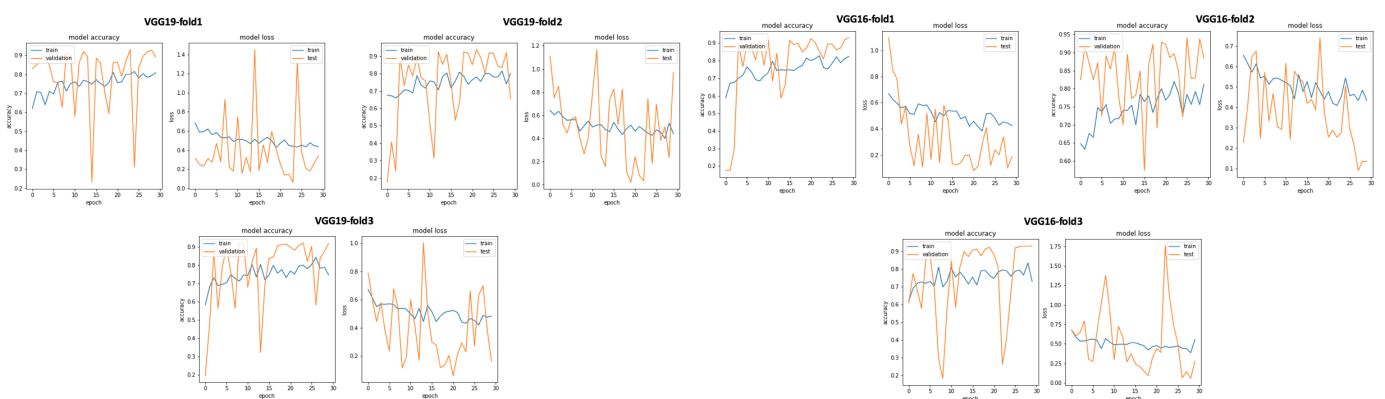


**Figure 25.** VGG19 and VGG16 training and validation curves using data selection based on clustering.

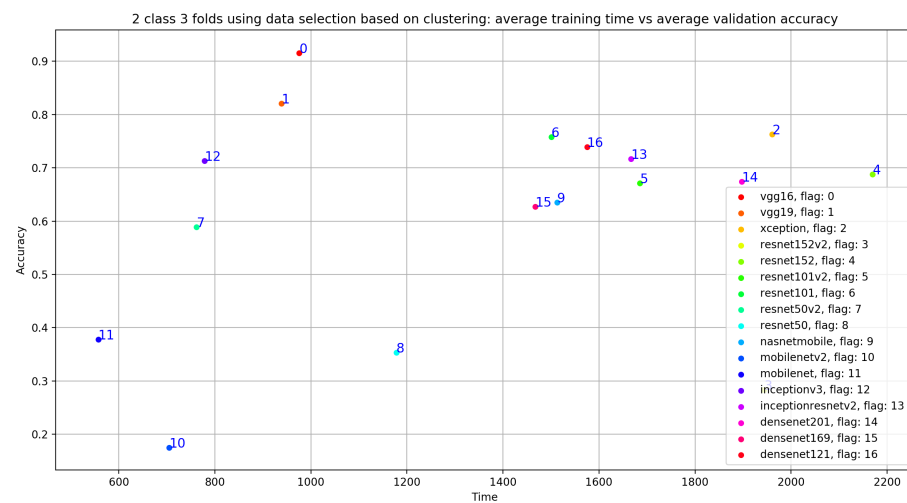


Figure 26. Training time vs. validation accuracy using data selection based on clustering.

Table 6. Average metric results related to clustered dataset.

Average	Accuracy	TPR (Sensitivity)	Precision (PPV)	TNR (Specificity)
<b>VGG16</b>	<b>0.915</b>	<b>0.873</b>	<b>0.860</b>	<b>0.873</b>
<b>VGG19</b>	0.821	0.808	0.787	0.808
<b>Xception</b>	0.763	0.795	0.690	0.795
<b>ResNet152V2</b>	0.283	0.561	0.590	0.561
<b>ResNet152</b>	0.688	0.712	0.728	0.712
<b>ResNet101V2</b>	0.671	0.702	0.674	0.702
<b>ResNet101</b>	0.758	0.765	0.682	0.765
<b>ResNet50v2</b>	0.589	0.666	0.633	0.666
<b>ResNet50</b>	0.353	0.576	0.396	0.576
<b>NasNetMobile</b>	0.635	0.498	0.561	0.498
<b>MobileNetV2</b>	0.175	0.500	0.195	0.500
<b>MobileNet</b>	0.378	0.606	0.422	0.606
<b>Inceptionv3</b>	0.713	0.773	0.668	0.773
<b>InceptionResNetV2</b>	0.717	0.717	0.761	0.717
<b>DenseNet201</b>	0.674	0.746	0.672	0.746
<b>DenseNet169</b>	0.627	0.758	0.656	0.758
<b>DenseNet121</b>	0.739	0.683	0.762	0.683

### 5.2.2. Synthesis

We have undergone a general comparative study against the state-of-the-art methods, as summarized in Table 7. As seen in this table, Dominguez et al. [60] achieved good classification results (accuracy of 0.97, sensitivity of 0.93, specificity of 0.95) using a complex recognition methodology based on heartbeat segmentation and a modified version of the CNN AlexNet model. Philip et al. [61] obtained the worst classification results in Table 7, and this is due to the elimination of the complex heart-cycle segmentation step. The majority of the research work presented in this table employed complex segmentation steps in their classification approach, and they obtained accuracy varying from 0.80 to 0.97, sensitivity from 0.76 to 0.96, and specificity from 0.72 to 0.95. In this work, our main contribution is to obtain very good classification results using a simple classification approach without any complex preprocessing steps, without any segmentation process,

and without the use of any new CNN architecture. As seen in Table 7, compared to the work of Dominguez et al. [60], we have achieved similar results with an accuracy equal to 0.97, a slightly better sensitivity result of 0.946, and a slightly lower specificity result of 0.946.

**Table 7.** Comparative analysis of our method with state-of-the-art methods using whole datasets from PhysioNet 2016.

Average	Accuracy	TPR (Sensitivity)	Precision (PPV)	TNR (Specificity)
<b>our approach</b>	<b>0.970</b>	<b>0.946</b>	<b>0.944</b>	<b>0.946</b>
[62]	0.8697	0.964	-	0.726
[17]	-	0.942	-	0.778
[63]	0.824	-	-	-
[18]	-	0.8095	-	0.839
[16]	-	0.84	-	0.957
[64]	0.852	-	-	-
[65]	-	0.885	-	0.921
[20]	0.879	0.885	-	0.878
[60]	0.97	0.932	-	0.951
[66]	0.915	0.983	-	0.846
[67]	0.892	0.90	-	0.884
[68]	0.88	0.88	-	0.87
[69]	0.85	0.89	-	0.816
[70]	0.826	0.769	-	0.883
[71]	0.801	0.796	-	0.806
[72]	0.9	0.93	-	0.9
[61]	0.79	0.77	-	0.8

## 6. Conclusions and Perspectives

In this work, we presented a simple classification architecture based on a data-selection process designed to recognize normal and abnormal Physionet PCG signals. We compared our work with the state-of-the-art approaches and concluded that using a data selection process based on a signal duration of 20 s for normal and 35 s for abnormal PCG signals obtained very good CNN classification results with an overall accuracy equal to 0.97, an overall sensitivity equal to 0.946, an overall precision equal to 0.944, an overall specificity equal to 0.946. This work was tested only on the most-used binary class dataset Physionet, which can be considered as a limiting factor. We plan to test it on other public or private multiclass datasets. In addition, the feature-selection process can be improved through the exploitation of a large set of ML feature extraction/selection methods. Furthermore, we plan to create our own multiclass PCG dataset which will be trained on a new CNN model created especially for PCG spectrogram images.

**Author Contributions:** Conceptualization, A.B. and M.B.; methodology, A.B., M.B. and R.S.; software, M.B. and R.S.; validation, A.B. and M.B.; formal analysis, M.B. and R.S.; investigation, A.B. and M.B.; writing—original draft preparation, A.B., M.B. and R.S.; writing—review and editing, M.B. and A.B.; supervision, A.B.; project administration, A.B. and M.B. All authors have read and agreed to the published version of the manuscript.

**Funding:** This research work was funded by Institutional Fund Projects under grant no (IFPIP: 574-611-1442). Therefore, the authors gratefully acknowledge technical and financial support from the Ministry of Education and King Abdelaziz University, DSR, Jeddah, Saudi Arabia.

**Institutional Review Board Statement:** Not applicable.

**Informed Consent Statement:** Not applicable.

**Data Availability Statement:** Not applicable.

**Acknowledgments:** This research work was funded by Institutional Fund Projects under grant no (IFPIP: 574-611-1442). Therefore, the authors gratefully acknowledge technical and financial support from the Ministry of Education and King Abdelaziz University, DSR, Jeddah, Saudi Arabia.

**Conflicts of Interest:** The authors declare no conflict of interest.

## References

- World Health Organization World Health Ranking. 2020. Available online: [https://www.who.int/health-topics/cardiovascular-diseases#tab=tab\\_1](https://www.who.int/health-topics/cardiovascular-diseases#tab=tab_1) (accessed on 15 February 2021).
- Yang, Z.J.; Liu, J.; Ge, J.P.; Chen, L.; Zhao, Z.G.; Yang, W.Y. Prevalence of Cardiovascular Disease Risk Factor in the Chinese Population: The 2007–2008 China National Diabetes and Metabolic Disorders Study. *Eur. Heart J.* **2011**, *33*, 213–220. [[CrossRef](#)] [[PubMed](#)]
- Mangione, S.; Nieman, L.Z. Cardiac Auscultatory Skills of Internal Medicine and Family Practice Trainees: A Comparison of Diagnostic Proficiency. *JAMA* **1997**, *278*, 717–722. [[CrossRef](#)] [[PubMed](#)]
- Lam, M.; Lee, T.; Boey, P.; Ng, W.; Hey, H.; Ho, K.; Cheong, P. Factors influencing cardiac auscultation proficiency in physician trainees. *Singap. Med. J.* **2005**, *46*, 11–14.
- Roelandt, J. The decline of our physical examination skills: Is echocardiography to blame? *Eur. Heart J. Cardiovasc. Imaging* **2013**, *15*, 249–252. [[CrossRef](#)]
- Grzegorzczak, I.; Soliński, M.; Łeppek, M.; Perka, A.; Rosiński, J.; Rymko, J.; Stępień, K.; Gierałowski, J. PCG classification using a neural network approach. In Proceedings of the 2016 Computing in Cardiology Conference (CinC), Vancouver, BC, Canada, 11–14 September 2016; pp. 1129–1132.
- Liu, C.; Springer, D.; Li, Q.; Moody, B.; Juan, R.A.; Chorro, F.J.; Castells, F.; Roig, J.M.; Silva, I.; Johnson, A.E.; et al. An open access database for the evaluation of heart sound algorithms. *Physiol. Meas.* **2016**, *37*, 2181. [[CrossRef](#)]
- Nouraei, H.; Nouraei, H.; Rabkin, S.W. Comparison of Unsupervised Machine Learning Approaches for Cluster Analysis to Define Subgroups of Heart Failure with Preserved Ejection Fraction with Different Outcomes. *Bioengineering* **2022**, *9*, 175. [[CrossRef](#)]
- Aruleba, R.T.; Adekiya, T.A.; Ayawei, N.; Obaido, G.; Aruleba, K.; Mienye, I.D.; Aruleba, I.; Ogbuokiri, B. COVID-19 Diagnosis: A Review of Rapid Antigen, RT-PCR and Artificial Intelligence Methods. *Bioengineering* **2022**, *9*, 153. [[CrossRef](#)]
- Elaziz, M.A.; Hosny, K.M.; Salah, A.; Darwish, M.M.; Lu, S.; Sahlol, A.T. New machine learning method for image-based diagnosis of COVID-19. *PLoS ONE* **2020**, *15*, e0235187. [[CrossRef](#)]
- Magar, R.; Yadav, P.; Barati Farimani, A. Potential neutralizing antibodies discovered for novel corona virus using machine learning. *Sci. Rep.* **2021**, *11*, 5261. [[CrossRef](#)]
- Sujath, R.A.A.; Chatterjee, J.M.; Hassani, A.E. A machine learning forecasting model for COVID-19 pandemic in India. *Stoch. Environ. Res. Risk Assess.* **2020**, *34*, 959–972. [[CrossRef](#)]
- Chintalapudi, N.; Battineni, G.; Hossain, M.A.; Amenta, F. Cascaded Deep Learning Frameworks in Contribution to the Detection of Parkinson’s Disease. *Bioengineering* **2022**, *9*, 116. [[CrossRef](#)] [[PubMed](#)]
- Clifford, G.D.; Liu, C.; Moody, B.; Springer, D.; Silva, I.; Li, Q.; Mark, R.G. Classification of normal/abnormal heart sound recordings: The PhysioNet/Computing in Cardiology Challenge 2016. In Proceedings of the 2016 Computing in Cardiology Conference (CinC), Vancouver, BC, Canada, 11–14 September 2016; pp. 609–612.
- Nogueira, D.M.; Ferreira, C.A.; Gomes, E.F.; Jorge, A.M. Classifying heart sounds using images of motifs, MFCC and temporal features. *J. Med. Syst.* **2019**, *43*, 168. [[CrossRef](#)] [[PubMed](#)]
- Rubin, J.; Abreu, R.; Ganguli, A.; Nelaturi, S.; Matei, I.; Sricharan, K. Recognizing abnormal heart sounds using deep learning. *arXiv* **2017**, arXiv:1707.04642.
- Potes, C.; Parvaneh, S.; Rahman, A.; Conroy, B. Ensemble of feature-based and deep learning-based classifiers for detection of abnormal heart sounds. In Proceedings of the 2016 Computing in Cardiology Conference (CinC), Vancouver, BC, Canada, 11–14 September 2016; pp. 621–624.
- Tang, H.; Chen, H.; Li, T.; Zhong, M. Classification of normal/abnormal heart sound recordings based on multi-domain features and back propagation neural network. In Proceedings of the 2016 Computing in Cardiology Conference (CinC), Vancouver, BC, Canada, 11–14 September 2016; pp. 593–596.
- Kiranyaz, S.; Zabihi, M.; Rad, A.B.; Ince, T.; Hamila, R.; Gabbouj, M. Real-time Phonocardiogram Anomaly Detection by Adaptive 1D Convolutional Neural Networks. *Neurocomputing* **2020**, *411*, 291–301. [[CrossRef](#)]
- Singh, S.A.; Majumder, S. Short unsegmented PCG classification based on ensemble classifier. *Turk. J. Electr. Eng. Comput. Sci.* **2020**, *28*, 875–889. [[CrossRef](#)]
- Krishnan, P.T.; Balasubramanian, P.; Umamathy, S. Automated heart sound classification system from unsegmented phonocardiogram (PCG) using deep neural network. *Phys. Eng. Sci. Med.* **2020**, *43*, 505–515. [[CrossRef](#)]

22. Garg, V.; Mathur, A.; Mangla, N.; Rawat, A.S. Heart Rhythm Abnormality Detection from PCG Signal. In Proceedings of the 2019 Twelfth International Conference on Contemporary Computing (IC3), Noida, India, 8–10 August 2019; pp. 1–5.
23. Alaskar, H.; Alzhrani, N.; Hussain, A.; Almarshed, F. The Implementation of Pretrained AlexNet on PCG Classification. In Proceedings of the International Conference on Intelligent Computing, Nanchang, China, 3–6 August 2019; pp. 784–794.
24. Khaled, S.; Fakhry, M.; Mubarak, A.S. Classification of PCG Signals Using A Nonlinear Autoregressive Network with Exogenous Inputs (NARX). In Proceedings of the 2020 International Conference on Innovative Trends in Communication and Computer Engineering (ITCE), Aswan, Egypt, 8–9 February 2020; pp. 98–102.
25. Noman, F.; Ting, C.M.; Salleh, S.H.; Ombao, H. Short-segment heart sound classification using an ensemble of deep convolutional neural networks. In Proceedings of the ICASSP 2019—2019 IEEE International Conference on Acoustics, Speech and Signal Processing (ICASSP), Brighton, UK, 12–17 May 2019; pp. 1318–1322.
26. Parzen, E. On estimation of a probability density function and mode. *Ann. Math. Stat.* **1962**, *33*, 1065–1076. [[CrossRef](#)]
27. Hoult, D.I.; Richards, R. The signal-to-noise ratio of the nuclear magnetic resonance experiment. *J. Magn. Reson.* (1969) **1976**, *24*, 71–85. [[CrossRef](#)]
28. McLachlan, G.; Peel, D. *Finite Mixture Models*; John Wiley & Sons: Hoboken, NJ, USA, 2004.
29. McLachlan, G.; Krishnan, T. *The EM Algorithm and Extensions*; John Wiley & Sons: Hoboken, NJ, USA, 2007; Volume 382.
30. Bishop, C.M. *Pattern Recognition and Machine Learning*; Springer: Berlin/Heidelberg, Germany, 2006.
31. Hastie, T.; Tibshirani, R.; Friedman, J.; Franklin, J. The elements of statistical learning: Data mining, inference and prediction. *Math. Intell.* **2005**, *27*, 83–85.
32. Fayek, H.M. Speech Processing for Machine Learning: Filter Banks, Mel Frequency Cepstral Coefficients (MFCCs) and What's In-Between. 2016. Available online: <https://haythamfayek.com/2016/04/21/speech-processing-for-machine-learning.html> (accessed on 15 February 2021).
33. Dave, N. Feature extraction methods LPC, PLP and MFCC in speech recognition. *Int. J. Adv. Res. Eng. Technol.* **2013**, *1*, 1–4.
34. Han, W.; Chan, C.F.; Choy, C.S.; Pun, K.P. An efficient MFCC extraction method in speech recognition. In Proceedings of the 2006 IEEE International Symposium on Circuits and Systems, Kos, Greece, 21–24 May 2006; p. 4.
35. Al Marzuqi, H.M.O.; Hussain, S.M.; Frank, A. Device Activation based on Voice Recognition using Mel Frequency Cepstral Coefficients (MFCC's) Algorithm. *Int. Res. J. Eng. Technol.* **2019**, *6*, 4297–4301.
36. Milletari, F.; Ahmadi, S.A.; Kroll, C.; Plate, A.; Rozanski, V.; Maiostre, J.; Levin, J.; Dietrich, O.; Ertl-Wagner, B.; Bötzel, K.; et al. Hough-CNN: Deep learning for segmentation of deep brain regions in MRI and ultrasound. *Comput. Vis. Image Underst.* **2017**, *164*, 92–102. [[CrossRef](#)]
37. Bar, Y.; Diamant, I.; Wolf, L.; Lieberman, S.; Konen, E.; Greenspan, H. Chest pathology detection using deep learning with non-medical training. In Proceedings of the 2015 IEEE 12th International Symposium On Biomedical Imaging (ISBI), Brooklyn, NY, USA, 16–19 April 2015; pp. 294–297.
38. Yan, L.; Yoshua, B.; Geoffrey, H. Deep learning. *Nature* **2015**, *521*, 436–444.
39. Li, W.; Wu, G.; Du, Q. Transferred deep learning for anomaly detection in hyperspectral imagery. *IEEE Geosci. Remote. Sens. Lett.* **2017**, *14*, 597–601. [[CrossRef](#)]
40. LeCun, Y.; Bottou, L.; Bengio, Y.; Haffner, P. Gradient-based learning applied to document recognition. *Proc. IEEE* **1998**, *86*, 2278–2324. [[CrossRef](#)]
41. Jiang, H.; Learned-Miller, E. Face detection with the faster R-CNN. In Proceedings of the 2017 12th IEEE International Conference on Automatic Face & Gesture Recognition (FG 2017), Washington, DC, USA, 30 May–3 June 2017; pp. 650–657.
42. Zhu, C.; Zheng, Y.; Luu, K.; Savvides, M. Cms-rnn: Contextual multi-scale region-based cnn for unconstrained face detection. In *Deep Learning for Biometrics*; Springer: Berlin/Heidelberg, Germany, 2017; pp. 57–79.
43. Li, H.; Lin, Z.; Shen, X.; Brandt, J.; Hua, G. A convolutional neural network cascade for face detection. In Proceedings of the IEEE Conference on Computer Vision and Pattern Recognition, Boston, MA, USA, 7–12 June 2015; pp. 5325–5334.
44. Niu, X.X.; Suen, C.Y. A novel hybrid CNN—SVM classifier for recognizing handwritten digits. *Pattern Recognit.* **2012**, *45*, 1318–1325. [[CrossRef](#)]
45. Matsumoto, T.; Chua, L.O.; Suzuki, H. CNN cloning template: Connected component detector. *IEEE Trans. Circuits Syst.* **1990**, *37*, 633–635. [[CrossRef](#)]
46. Wu, C.; Fan, W.; He, Y.; Sun, J.; Naoi, S. Handwritten character recognition by alternately trained relaxation convolutional neural network. In Proceedings of the 2014 14th International Conference on Frontiers in Handwriting Recognition, Crete Island, Greece, 1–4 September 2014; pp. 291–296.
47. Wang, J.; Yang, Y.; Mao, J.; Huang, Z.; Huang, C.; Xu, W. Cnn-rnn: A unified framework for multi-label image classification. In Proceedings of the IEEE Conference on Computer Vision and Pattern Recognition, Las Vegas, NV, USA, 27–30 June 2016; pp. 2285–2294.
48. Lee, H.; Kwon, H. Going deeper with contextual CNN for hyperspectral image classification. *IEEE Trans. Image Process.* **2017**, *26*, 4843–4855. [[CrossRef](#)]
49. Yu, S.; Jia, S.; Xu, C. Convolutional neural networks for hyperspectral image classification. *Neurocomputing* **2017**, *219*, 88–98. [[CrossRef](#)]
50. Tan, C.; Sun, F.; Kong, T.; Zhang, W.; Yang, C.; Liu, C. A survey on deep transfer learning. In Proceedings of the International Conference on Artificial Neural Networks, Rhodes, Greece, 4–7 October 2018; pp. 270–279.

51. Chollet, F. Xception: Deep learning with depthwise separable convolutions. In Proceedings of the IEEE Conference on Computer Vision and Pattern Recognition, Honolulu, HI, USA, 21–26 June 2017; pp. 1251–1258.
52. Simonyan, K.; Zisserman, A. Very deep convolutional networks for large-scale image recognition. *arXiv* **2014**, arXiv:1409.1556.
53. He, K.; Zhang, X.; Ren, S.; Sun, J. Deep residual learning for image recognition. In Proceedings of the IEEE Conference on Computer Vision and Pattern Recognition, Las Vegas, NV, USA, 27–30 June 2016; pp. 770–778.
54. Zoph, B.; Vasudevan, V.; Shlens, J.; Le, Q.V. Learning transferable architectures for scalable image recognition. In Proceedings of the IEEE Conference on Computer Vision and Pattern Recognition, Salt Lake City, UT, USA, 18–22 June 2018; pp. 8697–8710.
55. Sandler, M.; Howard, A.; Zhu, M.; Zhmoginov, A.; Chen, L.C. Mobilenetv2: Inverted residuals and linear bottlenecks. In Proceedings of the IEEE Conference on Computer Vision and Pattern Recognition, Salt Lake City, UT, USA, 18–22 June 2018; pp. 4510–4520.
56. Howard, A.G.; Zhu, M.; Chen, B.; Kalenichenko, D.; Wang, W.; Weyand, T.; Andreetto, M.; Adam, H. Mobilenets: Efficient convolutional neural networks for mobile vision applications. *arXiv* **2017**, arXiv:1704.04861.
57. Szegedy, C.; Vanhoucke, V.; Ioffe, S.; Shlens, J.; Wojna, Z. Rethinking the inception architecture for computer vision. In Proceedings of the IEEE Conference on Computer Vision and Pattern Recognition, Las Vegas, NV, USA, 27–30 June 2016; pp. 2818–2826.
58. Szegedy, C.; Ioffe, S.; Vanhoucke, V.; Alemi, A.A. Inception-v4, inception-resnet and the impact of residual connections on learning. In Proceedings of the Thirty-First AAAI Conference on Artificial Intelligence, San Francisco, CA, USA, 4–9 February 2017.
59. Huang, G.; Liu, Z.; Van Der Maaten, L.; Weinberger, K.Q. Densely connected convolutional networks. In Proceedings of the IEEE Conference on Computer Vision and Pattern Recognition, Honolulu, HI, USA, 21–26 June 2017; pp. 4700–4708.
60. Dominguez-Morales, J.P.; Jimenez-Fernandez, A.F.; Dominguez-Morales, M.J.; Jimenez-Moreno, G. Deep neural networks for the recognition and classification of heart murmurs using neuromorphic auditory sensors. *IEEE Trans. Biomed. Circuits Syst.* **2017**, *12*, 24–34. [[CrossRef](#)] [[PubMed](#)]
61. Langley, P.; Murray, A. Heart sound classification from unsegmented phonocardiograms. *Physiol. Meas.* **2017**, *38*, 1658. [[CrossRef](#)] [[PubMed](#)]
62. Nogueira, D.M.; Ferreira, C.A.; Jorge, A.M. Classifying heart sounds using images of MFCC and temporal features. In Proceedings of the EPIA Conference on Artificial Intelligence, Porto, Portugal, 5–8 September 2017; pp. 186–203.
63. Ortiz, J.J.G.; Phoo, C.P.; Wiens, J. Heart sound classification based on temporal alignment techniques. In Proceedings of the 2016 Computing in Cardiology Conference (CinC), Vancouver, BC, Canada, 11–14 September 2016; pp. 589–592.
64. Kay, E.; Agarwal, A. DropConnected neural networks trained on time-frequency and inter-beat features for classifying heart sounds. *Physiol. Meas.* **2017**, *38*, 1645. [[CrossRef](#)] [[PubMed](#)]
65. Abdollahpur, M.; Ghiasi, S.; Mollakazemi, M.J.; Ghaffari, A. Cycle selection and neuro-voting system for classifying heart sound recordings. In Proceedings of the 2016 Computing in Cardiology Conference (CinC), Vancouver, BC, Canada, 11–14 September 2016; pp. 1–4.
66. Han, W.; Yang, Z.; Lu, J.; Xie, S. Supervised threshold-based heart sound classification algorithm. *Physiol. Meas.* **2018**, *39*, 115011. [[CrossRef](#)] [[PubMed](#)]
67. Whitaker, B.M.; Suresha, P.B.; Liu, C.; Clifford, G.D.; Anderson, D.V. Combining sparse coding and time-domain features for heart sound classification. *Physiol. Meas.* **2017**, *38*, 1701. [[CrossRef](#)] [[PubMed](#)]
68. Tang, H.; Dai, Z.; Jiang, Y.; Li, T.; Liu, C. PCG classification using multidomain features and SVM classifier. *Biomed Res. Int.* **2018**, *2018*, 4205027. [[CrossRef](#)]
69. Plesinger, F.; Viscor, I.; Halamek, J.; Jurco, J.; Jurak, P. Heart sounds analysis using probability assessment. *Physiol. Meas.* **2017**, *38*, 1685. [[CrossRef](#)]
70. Abdollahpur, M.; Ghaffari, A.; Ghiasi, S.; Mollakazemi, M.J. Detection of pathological heart sounds. *Physiol. Meas.* **2017**, *38*, 1616. [[CrossRef](#)]
71. Homsy, M.N.; Warrick, P. Ensemble methods with outliers for phonocardiogram classification. *Physiol. Meas.* **2017**, *38*, 1631. [[CrossRef](#)]
72. Singh, S.A.; Majumder, S. Classification of unsegmented heart sound recording using KNN classifier. *J. Mech. Med. Biol.* **2019**, *19*, 1950025. [[CrossRef](#)]

**Disclaimer/Publisher’s Note:** The statements, opinions and data contained in all publications are solely those of the individual author(s) and contributor(s) and not of MDPI and/or the editor(s). MDPI and/or the editor(s) disclaim responsibility for any injury to people or property resulting from any ideas, methods, instructions or products referred to in the content.